Athens Journal of Sciences

Quarterly Academic Periodical, Volume 11, Issue 4, December 2024
URL: https://www.athensjournals.gr/ajs
Email: journals@atiner.gr
e-ISSN: 2241-8466 DOI: 10.30958/ajs

Front Pages

Athens Journal of Sciences

Published by the Athens Institute for Education and Research (ATINER)

****

ATINER is an Athens-based World Association of Academics and Researchers based in Athens. ATINER is an independent and non-profit Association with a Mission to become a forum where Academics and Researchers from all over the world can meet in Athens, exchange ideas on their research and discuss future developments in their disciplines, as well as engage with professionals from other fields. Athens was chosen because of its long history of academic gatherings, which go back thousands of years to Plato's Academy and Aristotle's Lyceum. Both these historic places are within walking distance from ATINER's downtown offices. Since antiquity, Athens was an open city. In the words of Pericles, Athens"…is open to the world, we never expel a foreigner from learning or seeing". ("Pericles' Funeral Oration", in Thucydides, The History of the Peloponnesian War). It is ATINER's mission to revive the glory of Ancient Athens by inviting the World Academic Community to the city, to learn from each other in an environment of freedom and respect for other people's opinions and beliefs. After all, the free expression of one's opinion formed the basis for the development of democracy, and Athens was its cradle. As it turned out, the Golden Age of Athens was in fact, the Golden Age of the Western Civilization. Education and (Re)searching for the 'truth' are the pillars of any free (democratic) society. This is the reason why Education and Research are the two core words in ATINER's name.

****

The ***Athens Journal of Sciences (AJS)*** is an Open Access quarterly double-blind peer reviewed journal and considers papers from all areas of Natural & Formal Sciences, including papers on agriculture, computer science, environmental science, materials science, transportation science, chemistry, physics, mathematics and statistics, biology, geography, and earth science (geology, oceanography, astronomy, meteorology). Many of the papers published in this journal have been presented at the various conferences sponsored by the Natural & Formal Sciences Division of the Athens Institute for Education and Research (ATINER). All papers are subject to ATINER's Publication Ethical Policy and Statement.

The Athens Journal of Sciences
ISSN NUMBER: 2241-8466- DOI: 10.30958/ajs
Volume 11, Issue 4, December 2024
Download the entire issue (PDF)

Athens Journal of Sciences
Editorial and Reviewers' Board

President's Message

All ATINER's publications including its e-journals are open access without any costs (submission, processing, publishing, open access paid by authors, open access paid by readers etc.) and is independent of presentations at any of the many small events (conferences, symposiums, forums, colloquiums, courses, roundtable discussions) organized by ATINER throughout the year and entail significant costs of participating. The intellectual property rights of the submitting papers remain with the author. Before you submit, please make sure your paper meets the basic academic standards, which includes proper English. Some articles will be selected from the numerous papers that have been presented at the various annual international academic conferences organized by the different divisions and units of the Athens Institute for Education and Research. The plethora of papers presented every year will enable the editorial board of each journal to select the best, and in so doing produce a top-quality academic journal. In addition to papers presented, ATINER will encourage the independent submission of papers to be evaluated for publication.

The current issue is the fourth of the eleventh volume of the *Athens Journal of Sciences (AJS),* published by Natural & Formal Sciences Division of ATINER.

Gregory T. Papanikos, President, ATINER.

Athens Institute for Education and Research

A World Association of Academics and Researchers

13th Annual International Conference on Chemistry
21-24 July 2025, Athens, Greece

The Natural Sciences Unit of ATINER, will hold its **13th Annual International Conference on Chemistry, 21-24 July 2025, Athens, Greece** sponsored by the Athens Journal of Sciences. The aim of the conference is to bring together academics and researchers of all areas of chemistry and other related disciplines. You may participate as stream organizer, presenter of one paper, chair a session or observer. Please submit a proposal using the form available (https://www.atiner.gr/2025/FORM-CHE.doc).

Academic Members Responsible for the Conference

- **Dr. Haiduke Sarafian**, Head, Natural Sciences Unit, ATINER & Professor of Physics and Endowed Chair of John T. and Paige S. Smith Professor of Science, Pennsylvania State University, USA.

Important Dates

- Abstract Submission: **17 December 2024**
- Acceptance of Abstract: 4 Weeks after Submission
- Submission of Paper: **23 June 2025**

Social and Educational Program

The Social Program Emphasizes the Educational Aspect of the Academic Meetings of Atiner.

- Greek Night Entertainment (This is the official dinner of the conference)
- Athens Sightseeing: Old and New-An Educational Urban Walk
- Social Dinner
- Mycenae Visit
- Exploration of the Aegean Islands
- Delphi Visit
- Ancient Corinth and Cape Sounion

Conference Fees

Conference fees vary from 400€ to 2000€
Details can be found at: https://www.atiner.gr/fees

Athens Institute for Education and Research
A World Association of Academics and Researchers

13th Annual International Conference on Physics
21-24 July 2025, Athens, Greece

The Natural Sciences Unit of ATINER, will hold its **13th Annual International Conference on Physics, 21-24 July 2025, Athens, Greece** sponsored by the Athens Journal of Sciences. The aim of the conference is to bring together academics and researchers of all areas of physics and other related disciplines. Please submit a proposal using the form available (https://www.atiner.gr/2025/FORM-PHY.doc).

Important Dates

- Abstract Submission: **17 December 2024**
- Acceptance of Abstract: 4 Weeks after Submission
- Submission of Paper: **23 June 2025**

Academic Member Responsible for the Conference

- **Dr. Haiduke Sarafian**, Head, Natural Sciences Unit, ATINER & Professor of Physics and Endowed Chair of John T. and Paige S. Smith Professor of Science, Pennsylvania State University, USA.

Social and Educational Program

The Social Program Emphasizes the Educational Aspect of the Academic Meetings of Atiner.

- Greek Night Entertainment (This is the official dinner of the conference)
- Athens Sightseeing: Old and New-An Educational Urban Walk
- Social Dinner
- Mycenae Visit
- Exploration of the Aegean Islands
- Delphi Visit
- Ancient Corinth and Cape Sounion

More information can be found here: https://www.atiner.gr/social-program

Conference Fees

Conference fees vary from 400€ to 2000€
Details can be found at: https://www.atiner.gr/fees

Athens Journal of Sciences- Volume 11, Issue 4, December 2024 – Pages 221-232

Adjusting the Balance between Alpha and Beta Risks in NN Classifiers

By Philippe Thomas[*], Marie-Christine Suhner[±] & Hind Bril El Haouzi[°]

This paper delves into classification tasks, where data is categorized into binary classes, such as fraudulent/non-fraudulent or sick/not sick as example. Employing a statistical approach, this task entails utilizing hypothesis testing. Tuning this test involves selecting an acceptable risk alpha (associated with false positives), thereby implicating a beta risk (related to false negatives). In classification challenges, the principal aim is to mitigate the misclassification rate. However, the determination of these two risks is not be discretionary but rather enforced by the learning process, particularly evident when employing neural networks. This paper seeks to propose a modification of the learning algorithm for multilayer perceptron aimed at effectively balancing these risks. This adaptation hinges on leveraging a weighted criterion to minimize errors, accounting for the signs of different error types. This methodology is assessed across two benchmarks: a simulated dataset and a genuine medical dataset.

Keywords: *neural network, multilayer perceptron, learning, classification, hypothesis test*

Introduction

A common challenge in various domains is the ability to confidently classify data into two exclusive classes. This is particularly relevant in fields such as fraud detection (O'Kelly 2004), IT security (Hänisch & Karg 2019), medical diagnosis (Guyatt et al. 1995), and banking loan approval (Hidayah & Saptarini 2019). Historically, a statistical approach has been employed to address such problems using hypothesis testing.

Hypothesis testing entails the evaluation of competing hypotheses regarding population characteristics, typically denoted as H0 (null hypothesis) and H1 (alternative hypothesis). This methodology introduces two potential errors: Type I error (alpha), representing the risk of falsely rejecting the null hypothesis H0, and Type II error (beta), indicating the risk of falsely accepting H0. The interrelation between these risks, alpha and beta, is notable; an increase in alpha risk leads to a decrease in beta risk and vice versa. Thus, the fundamental principle of statistical studies involves selecting an acceptable alpha risk to construct the test, facilitating risk management.

Another, more recent approach is to use machine learning tools, in particular neural networks, to solve these classification problems (Bao et al. 2022, Chandrasekaran

[*]Associate Professor, University of Lorraine, CRAN, France.
[±]Assistant Professor, University of Lorraine, CRAN, France.
[°]Professor, University of Lorraine, CRAN, France.

1983, Mytnyk et al. 2023, Joolfoo & Hosany 2023). However, these tools work differently. It involves defining a criterion to be minimized (generally the quadratic criterion) and using a criterion minimization algorithm (gradient backpropagation) to minimize the misclassification rate. The risks of false positives and false negatives are then imposed. This point is particularly critical when the data is poorly balanced, as in reliability studies where few data correspond to defects. In this case, these approaches lead to models that are biased in favor of the most represented class (Castro & Braga 2013). In extreme cases, a classification model that always assigns data to the same class will perform very well in terms of misclassification rate. To address this problem, cost-sensitive approaches have been proposed (Thomas 2015, Zadrozny et al. 2003, Zadrozny & Elkan 2001). However, these approaches still do not allow to control first- and second-species risks.

The main objective of this paper is to propose a modification of the learning algorithm based on a particular choice of the criterion to be minimized, exploiting the fact that the errors associated with a false alarm or non-detection are not of the same sign. A second objective is to illustrate the use of this approach in a medical context, in order to differentiate the treatment of patients according to the degree of confidence we have in the classification result.

In the next section, the structure of the multilayer perceptron used is described and the proposed learning algorithm is presented. Part 3 is dedicated to the presentation of the simulation example used to illustrate the performance of the algorithm. An application to a medical field is proposed and discussed in the following section before concluding.

Multilayer Perceptron

Structure

According to Cybenko (1989) and Funahashi (1989), a multilayer neural network that includes only one hidden layer with a sigmoidal activation function and an output layer can accurately approximate all nonlinear functions. For the sake of simplicity, we will only focus on the single output case in this presentation. However, it is important to note that the multi-output case can be derived from this scenario with ease. The equation for the network output $\hat{y}$ is defined as follows:

$$\hat{y} = g_o\left(\sum_{h=1}^{n_o} w_h^2 . g_h\left(\sum_{i=1}^{n_i} w_{hi}^1 . x_i + b_h^1\right) + b\right) \quad (1)$$

where x_i represents the n_i inputs, w_{hi}^1 represents the connecting weights between the input and hidden layers, b_h^1 represents the hidden neuron biases, $g_h(.)$ represents the activation function of the hidden neurons (hyperbolic tangent), w_h^2 represents the connecting weights between the hidden and output layers, b represents the bias of the output neuron, and $g_o(.)$ represents the activation function of the output neuron.

Because the problem at hand is a classification task, the sigmoidal function $g_o(.)$ was chosen. The accuracy of the model is heavily influenced by the initial parameter set due to the local search for minimum during MLP learning. Various initialization algorithms have been proposed in the past (Thomas & Bloch 1997). The modification of the Nguyen and Widrow (NW) algorithm (Nguyen & Widrow 1990) utilized in this study allows for a random initialization of weights and biases while to be optimally placed in the input space (Demuth et al. 1994).

Proposed learning Algorithm

The primary objective of the learning algorithm in a classification problem is to devise a model capable of correctly associating each pattern with its respective class. This model is directly derived from a training dataset. To achieve this, the goal is to minimize the mean square error between the predicted output of the model and the actual desired output. Therefore, the classical quadratic criterion to minimize is expressed as:

$$V(\theta) = \frac{1}{2n}\sum_{k=1}^{n} \varepsilon^2(k,\theta) \qquad (2)$$

where θ encompasses all the unknown network parameters (weights and biases), n is the size of the training dataset, and ε represents the prediction error or residual given by:

$$\varepsilon(k,\theta) = y(k) - \hat{y}(k,\theta) \qquad (3)$$

where $y(k)$ is the actual desired class of pattern k and $\hat{y}(k,\theta)$ is the predicted class by the network.

This criterion does not allow for adjusting the model based on the selected acceptable risks (alpha and beta). However, the sign of the residual ε(k,θ) provides information about the type of error. If hypothesis H0 (or H1) suggests that the data under consideration, k, belongs to class 0 (or class 1), then a residual of $\varepsilon(k,\theta) < 0$ corresponds to a false positive error (type I or alpha error), while a residual of $\varepsilon(k,\theta) > 0$ corresponds to a false-negative error (type II or beta error).

To utilize this information, the criterion to be minimized (2) can be modified by assigning weight $C_{\alpha\beta}(k)$ to the residual k based on its sign, giving more or less importance as necessary:

$$V(\theta) = \frac{1}{2n}\sum_{k=1}^{n} C_{\alpha\beta}(k).\varepsilon^2(k,\theta) \qquad (4)$$

where the weight is determined by:

$$\begin{cases} C_{\alpha\beta}(k) = C_\alpha & if \quad \varepsilon(k,\theta) < 0 \\ C_{\alpha\beta}(k) = C_\beta & if \quad \varepsilon(k,\theta) > 0 \end{cases} \qquad (5)$$

Here, C_α (or C_β) is a positive integer value that adjusts the influence of the considered residual $\varepsilon(k,\theta)$ if it corresponds to a type I error (or type II). Choosing C_α and C_β such that $C_\alpha > C_\beta$ (or $C_\alpha < C_\beta$) implies that the learned model will reduce the alpha risk (or beta risk). Setting $C_\alpha = C_\beta$ corresponds to the classical quadratic criterion (2).

The classical Gauss-Newton algorithm is obtained by the 2nd-order Taylor series expansion of the minimization criterion (4):

$$\hat{\theta}^{i+1} = \hat{\theta}^{i} - (H(\hat{\theta}^{i}))^{-1} V'(\hat{\theta}^{i}) \qquad (6)$$

where $\hat{\theta}^{i}$ is the set of network parameters estimated at iteration i, $V'(\hat{\theta}^{i})$ is the criterion gradient and $H(\hat{\theta}^{i})$ is the Hessian Matrix. The gradient of the criterion is given by:

$$V'(\theta) = -\frac{1}{n}\sum_{k=1}^{n} \psi(k,\theta).C_{\alpha\beta}(k).\varepsilon(k,\theta) \qquad (7)$$

where $\psi(k,\theta)$ is the gradient of $\hat{y}(k,\theta)$ with respect to q.

The Levenberg-Marquardt (Levenberg, 1944; Marquardt, 1963) update rule can be used to estimate the Hessian matrix:

$$H(\theta) = \frac{1}{n}\sum_{k=1}^{n} \psi(k,\theta).C_{\alpha\beta}(k).\psi^{T}(k,\theta) + \beta I \qquad (8)$$

where I is the identity matrix and β a small non negative scalar which must be adapted during the learning process.

Simulation Example

To demonstrate the proposed learning algorithm, we use a simple simulation example derived from the one proposed by (Lin et al. 2002). The example involves a population comprising two subpopulations. The positive subpopulation follows a bivariate normal distribution with a mean of $(0, 0)^T$ and a covariance matrix of diag(1, 1). On the other hand, the negative subpopulation follows two bivariate normal distributions. The first subpopulation has a mean of $(2, 2)^T$ with a covariance of diag(2, 1), while the second subpopulation has a mean of $(-2, -2)^T$ with a covariance of diag(2, 1). The population consists of a positive subpopulation and a negative subpopulation. The positive and negative subpopulations account for 80% and 20% of the total population, respectively. The subpopulation with negative values is balanced and follows two distinct laws to prevent linear separability of the two classes.

Figure 1 displays the distribution of the two classes in the space of the two inputs. The red circles represent class0, while the blue triangles represent class1. It is evident that these two classes are partially overlapping. This fact implies that even the most accurate classifier is unable to perform its task without producing misclassifications.

Figure 1. *Representation of the Simulation Dataset*

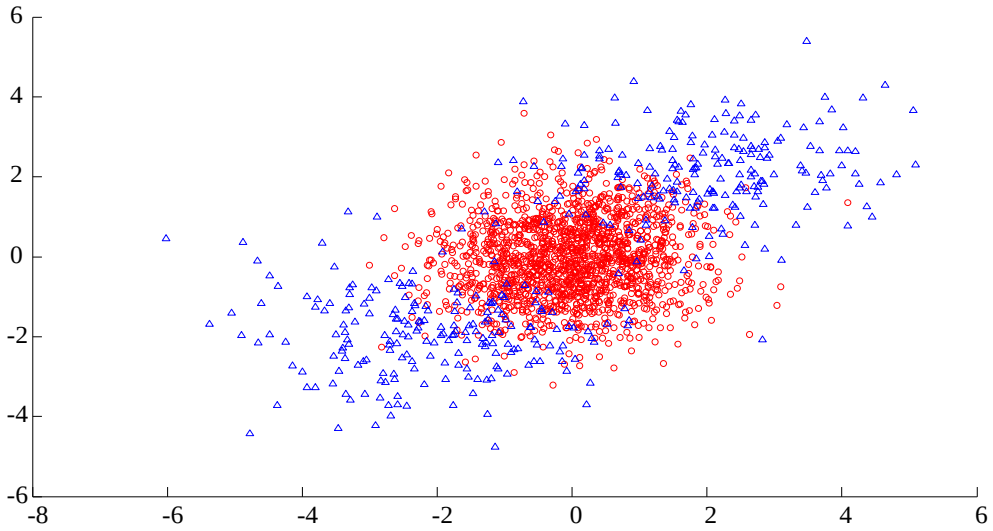

A dataset of 2,000 data points is generated based on the aforementioned distribution. The dataset is then randomly split into a training set and a validation set, each containing 1,000 data points. The training set is utilized to construct a neural classifier (MLP) with a structure consisting of 2 inputs and 10 hidden neurons, which is deemed appropriate for the problem. The size of the hidden layer was determined through a trial-and-error approach.

To prevent the issue of local minimum trapping, the training process utilizes 20 distinct sets of initial weights for each experience.

The misclassification rate, also known as the error rate or 'zero-one' score function (Hand et al. 2001), is the classical criterion for evaluating classifiers:

$$S_{01} = \frac{1}{n}\sum_{k=1}^{n} I(y(k), \hat{y}(k,\theta)) \quad (9)$$

where $I(a,b) = 1$ when $a \neq b$ and 0 otherwise.

Two other indicators must be determined: the false alarm rate (*FA*) and the non-detection rate (*ND*). These indicators are:

$$\begin{cases} FA = \frac{FP}{FP+TN} \\ ND = \frac{FN}{FN+TP} \end{cases} \quad (10)$$

where *FP* represents the number of false positives, *TN* represents the number of true negatives, *FN* represents the number of false negatives, and *TP* represents the number of true positives.

First, we will examine the effect of parameters choice on the misclassification rate. Specifically, we will focus on the impact of the C_α and C_β parameters (C_α =1 when $C_\beta \neq 1$ and vice versa) in equations 4 and 5. Figure 2 displays the dispersion

(boxplot) of misclassification rates obtained from 20 different sets of initial weights as the C_α/C_β ratio varies between 1/10 and 10.

Figure 2. *Boxplot of the S_{01} in Function of the C_α/C_β ratio for Simulation Example*

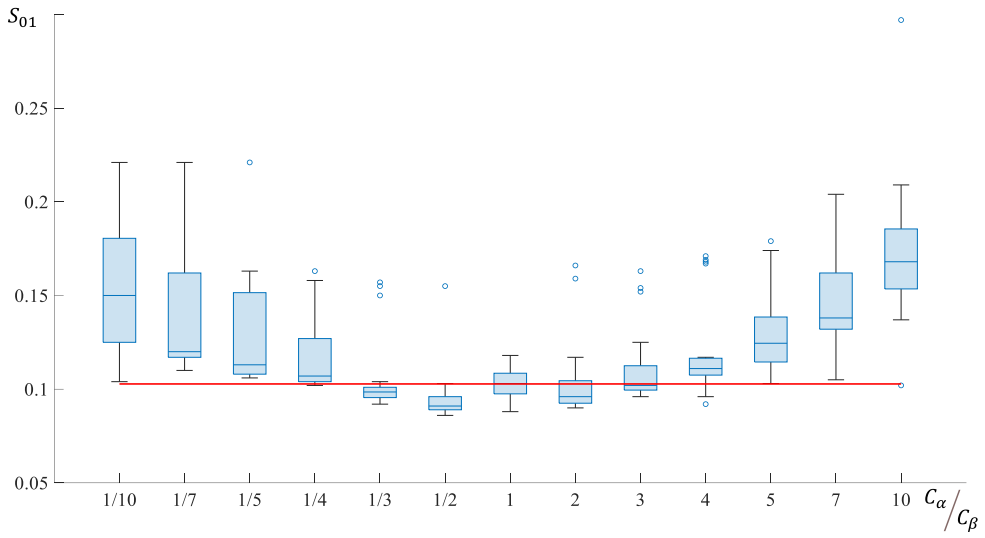

The reference model is the model that gives the lowest misclassification rate using the classical quadratic criterion ($C_\alpha/C_\beta = 1$). The results of all other models are compared with this model using a hypothesis test (proportion comparison) with a confidence level of 95%. The red line represents the acceptance limit of the test. Below this line, the considered model is statistically equivalent to the reference model; above this line, the considered model is statistically worse than the reference model. Figure 2 demonstrates that selecting a C_α/C_β ratio between 1/3 and 3 does not result in a decline in performance. In fact, for all boxplots analyzed, the median value remains below the red line, indicating that at least 50% of the models produce results that are statistically equivalent to those of the reference model. However, for values less than 1/3 or greater than 3, this statement no longer holds true. Therefore, it is important to make a reasonable choice for the C_α and C_β parameters and not exceed a value of 3.

Table 1 shows the rates (misclassification S_{01}, false alarm FA and non-detection ND) for the best model among the 20 trained with different C_α/C_β ratios obtained on the validation dataset. According to the results shown in figure 2, only ratios between 1/3 and 3 are shown.

The misclassification rates obtained with these five best models are statistically equivalent. Therefore, the proposed learning algorithm does not improve or degrade the misclassification rate. Additionally, a study of the false alarm rate (corresponding to the alpha risk) reveals that adjusting the C_α and C_β parameters can result in a range of rates between 1% and 7%. Similarly, adjusting

these same parameters can cause the non-detection rate (beta risk) to vary between 17% and 38%.

Table 1. *Misclassification, False Alarm and Non-detection Rates for the Best Models in Function of the* C_α / C_β *Ratio*

C_α/C_β	1/3	1/2	1	2	3
S_{01}	9.2%	8.6%	8.8%	9.0%	9.6%
FA (α risk)	0.9%	3.5%	3.7%	5.0%	7.6%
ND (β risk)	38.5%	26.7%	26.7%	23.1%	16.7%

Figure 3 displays the classification results obtained using two extreme models. The classification limits of the models are represented by a black curve for the model obtained with the ratio $C_\alpha/C_\beta = 3$ and a pink curve for the model obtained with the ratio $C_\alpha/C_\beta = 1/3$. Rounds represent data belonging to class 0, while triangles represent data belonging to class 1. The blue data points are well classified by both models, while the red data points are misclassified by both models. Data in green are those well classified by one model and misclassified by the other. It illustrates the usefulness of the proposed approach by defining three zones: a zone of high probability of belonging to class 0 (inside the black line), a zone of high probability of belonging to class 1 (outside the pink curve), and a zone of uncertainty between the two curves.

Figure 3. *Results of the Classification Models*

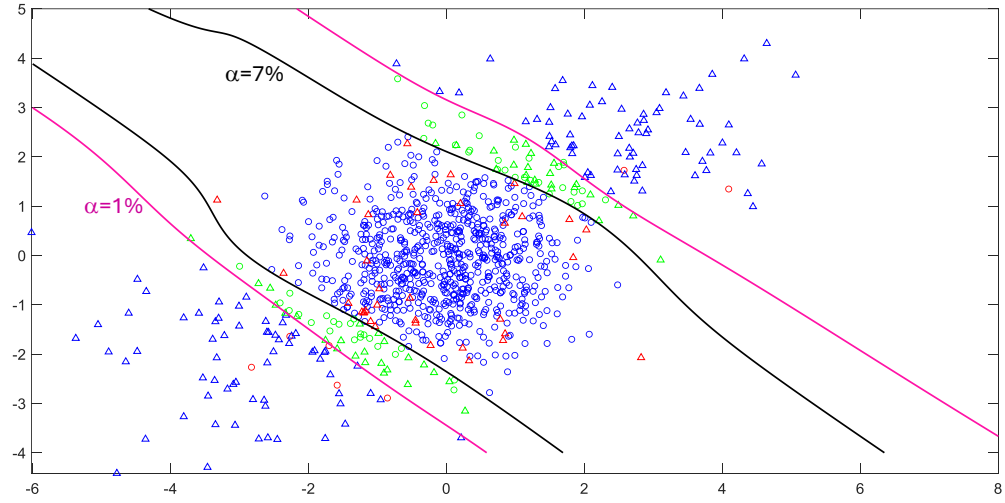

Medical Example

To illustrate the application of the approach, a medical example using a real dataset is presented. The dataset considered here concerns breast cancer diagnosis

(Mangasarian & Wolberg 1990) and can be downloaded from the UCI website[1]. This dataset includes 569 instances. For each instance, 11 variables are collected including the sample ID (not used here), the diagnosis (benign/malignant) which is the target of our model, and 9 features describing the tumor: clump thickness, uniformity of cell size, uniformity of cell shape, marginal adhesion, single epithelial cell size, bare nuclei, bland chromatin, normal nucleoli, mitoses, which are used as input of our model.

This dataset is subdivided into learning and validation datasets including 300 and 383 instances respectively (instances including missing data are removed).

The structure of the MLP used to learn this classification problem is composed of 9 inputs, 1 output and the size of the hidden layer is fitted to 5 neurons by using a trial-and-error strategy. As for the preceding example, to prevent the issue of local minimum trapping, the training process utilizes 20 distinct sets of initial weights for each experience.

Figure 4 is based on the same principle as figure 2. It shows the dispersion of misclassification rates obtained from 20 different sets of initial weights as the C_α / C_β ratio varies between 1/10 and 10. As for the figure 2, the reference model is the model that gives the lowest misclassification rate using the classical quadratic criterion ($C_\alpha / C_\beta = 1$). The results of all other models are compared with this model using a hypothesis test with a confidence level of 95% and the red line represents the acceptance limit of the test.

Figure 4 illustrates that the conventional quadratic criterion is not optimal in this context. In fact, the boxplot ($C_\alpha / C_\beta = 1$) reveals that over three-quarters of the models exhibit statistically inferior results relative to the reference model. Only the 1/4, 1/5, 1/7, and 1/10 ratios exhibit inferior performance in this regard. Furthermore, the impact of the C_α / C_β ratio is not symmetrical. Indeed, selecting $C_\alpha > C_\beta$ (alpha risk reduction) leads to markedly improved results (for ratios 2, 3, 4, and 5, more than half of the models are statistically equivalent to the reference model). Conversely, selecting the opposite choice leads to only about one quarter of the models being statistically equivalent to the reference model. This may be attributed to the fact that the data are slightly unbalanced (2/3 class 0; 1/3 class 1).

[1]https://archive.ics.uci.edu/dataset/15/breast+cancer+wisconsin+original.

Figure 4. *Boxplot of the S_{01} in Function of the C_α/C_β Ratio for Breast Cancer Problem*

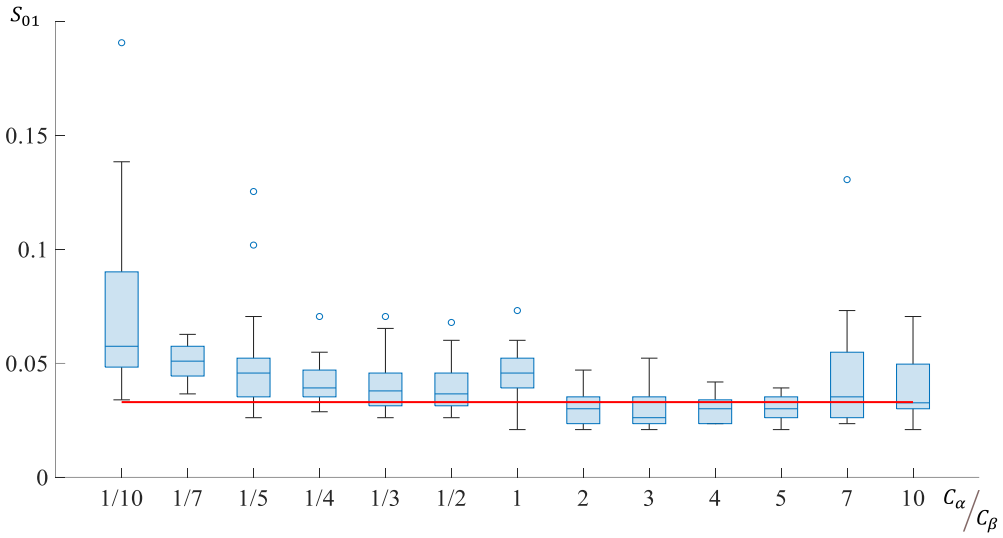

Table 2 shows the rates (misclassification S_{01}, false alarm FA and non-detection ND) for the best model among the 20 trained with different C_α/C_β ratios obtained on the validation dataset. As for the preceding case, only ratios between 1/3 and 3 are shown.

The misclassification rates obtained with these five best models are statistically equivalent. Therefore, the proposed learning algorithm does not improve or degrade the misclassification rate. Additionally, a study of the false alarm rate (corresponding to the alpha risk) reveals that adjusting the C_α and C_β parameters can result in a range of rates between 1.2% and 3%. Similarly, adjusting these same parameters can cause the non-detection rate (beta risk) to vary between 0% and 5%.

Table 2. *Misclassification, False Alarm and Non-detection Rates for the Best Models in Function of the C_α/C_β Ratio for Breast Cancer Problem*

C_α/C_β	1/3	1/2	1	2	3
S_{01}	2.6%	2.6%	2.1%	2.1%	2.1%
FA (α risk)	1.6%	1.2%	2.8%	2.8%	3.1%
ND (β risk)	4.7%	5.5%	0.8%	0.8%	0.0%

In a similar vein as illustrated Figure 3, it is possible to select two distinct models in order to differentiate treatments according to the cancer predictions provided by the two models. The two models selected here are the optimal models obtained with ratios of ½ and 3, respectively, and indicated in yellow in Table 2. The use of the ratio 3 model is particularly advantageous, as it offers a risk of non-detection of 0%. With this model, there is a high probability of correctly diagnosing all sick patients. Nevertheless, with this model, over 3% of cases are

false positives. In contrast, the model obtained with the ratio ½ leads to a non-detection rate of 5.5% but reduces the false positive rate to 1.2%. It is then possible to easily construct three groups of patients according to the results of these two models:

- Group 1: Patients declared healthy by both models. In this case, it can be assumed with a high degree of certainty that the patients are indeed healthy, and that regular follow-up will be sufficient.
- Group 2: Patients diagnosed with cancer by both models. In this case, the probability is very high that these patients do in fact have cancer, and treatment can begin very quickly.
- Group 3: Patients whose diagnose differ between the two models. In this instance, the risk of error is high, necessitating further investigations to refine the diagnosis.

Table 3 is derived from the confusion matrices. It presents the results obtained on the validation set by mapping predicted classes to actual classes. In comparison to a conventional confusion matrix, an additional column entitled "undetermined" is added, indicating the number of instances that are well classified by one model and poorly classified by the other. The "class 0" column corresponds to Group 1 of patients reported as not ill. Here, we find our non-detection rate of 0. The class 1 column corresponds to Group 2 of patients who were declared to have cancer. We note that only three of these patients were in fact healthy. The undetermined column corresponds to Group 3, which requires further investigation. This group includes almost as many healthy patients as cancer patients.

Table 3. *Modified Confusion Matrix*

		Predicted class		
		healthy	undetermined	cancer
real class	healthy	245	7	3
	cancer	0	10	118

Conclusion

This paper addresses the issue of two-class classification using neural networks, while controlling for first- and second-species risks. The primary concept is based on the use of a criterion to be minimized, including a weight that allows for the reduction of type I or type II errors to be given priority.

The proposed approach was tested on a simulation example where the impact of the choice of weight on the performance of the model learned in terms of misclassification, false alarm, and non-detection rates was evaluated. The results demonstrated that this weight favored a reduction in the number of false alarms or, conversely, non-detections, without compromising the misclassification rate. The

proposed algorithm was then tested on a medical dataset to illustrate the value of the approach in differentiating patient treatment according to diagnostic results.
One limitation of this approach that has not been addressed here is the potential impact of data pollution by outliers. Future work will be directed towards investigating the impact of outliers on the robustness of learned models.

Acknowledgments

This work was financially supported by the ANR-22-CE46-0010 JUNEAU.

References

Bao Y, Hilary G, Ke B (2022) Artificial Intelligence and Fraud Detection. In V Babich, JR Birge, G Hilary (eds.), *Innovative Technology at the Interface of Finance and Operations: Volume I*, 223–247. Springer International Publishing.

Castro CL, Braga AP (2013) Novel Cost-Sensitive Approach to Improve the Multilayer Perceptron Performance on Imbalanced Data. *IEEE Transactions on Neural Networks and Learning Systems* 24(6): 888–899.

Chandrasekaran B (1983) On Evaluating Artificial Intelligence Systems for Medical Diagnosis. *AI Magazine* 4(2): Article 2.

Cybenko G (1989) Approximation by superpositions of a sigmoidal function. *Mathematics of Control, Signals and Systems* 2(4): 303–314.

Demuth H, Beale M, Hagan M (1994) *Neural network toolbox*. Mathworks.

Funahashi K-I (1989) On the approximate realization of continuous mappings by neural networks. *Neural Networks* 2(3): 183–192.

Guyatt G, Jaeschke R, Heddle N, Cook D, Shannon H, Walter S (1995) Basic statistics for clinicians: 1. Hypothesis testing. *CMAJ: Canadian Medical Association Journal* 152(1): 27–32.

Hand D, Mannila H, Smyth P (2001) Principles of data mining. 2001. *MIT Press. Sections* 6(3): 2–6.

Hänisch T, Karg C (2019) Estimating the success of it security measures in industry 4.0 environments using monte carlo simulation on attack defense trees. *Athens Journal of Technology & Engineering* 6(4): 211–222.

Hidayah E, Saptarini GD (2019) Pentagon Fraud Analysis in Detecting Potential Financial Statement Fraud of Banking Companies in Indonesia. In *Proceeding UII-ICABE*, 89–102.

Joolfoo MBA, Hosany MA (2023) Machine learning solutions in combating COVID-19: State of the art and challenges. *Athens Journal of Technology* 10(1): 71–88.

Levenberg K (1944) A method for the solution of certain non-linear problems in least squares. *Quarterly of Applied Mathematics*.

Lin Y, Lee Y, Wahba G (2002) Support Vector Machines for Classification in Nonstandard Situations. *Machine Learning* 46(1): 191–202.

Mangasarian OL, Wolberg WH (1990) *Cancer diagnosis via linear programming*. University of Wisconsin-Madison Department of Computer Sciences.

Marquardt DW (1963) An Algorithm for Least-Squares Estimation of Nonlinear Parameters. *Journal of the Society for Industrial and Applied Mathematics* 11(2): 431–441.

Mytnyk B, Tkachyk O, Shakhovska N, Fedushko S, Syerov Y (2023) Application of Artificial Intelligence for Fraudulent Banking Operations Recognition. *Big Data and Cognitive Computing* 7(2): Article 2.

Nguyen D, Widrow B (1990) Improving the learning speed of 2-layer neural networks by choosing initial values of the adaptive weights. In *1990 IJCNN International Joint Conference on Neural Networks*, 21–26 volume 3.

O'Kelly M (2004) Using statistical techniques to detect fraud: A test case. *Pharmaceutical Statistics* 3(4): 237–246.

Thomas P (2015) Perceptron learning for classification problems: Impact of cost-sensitivity and outliers robustness | IEEE Conference Publication | IEEE Xplore. In *IJCCI'15 7th Int. Joint Conf. on Computational Intelligence*.

Thomas P, Bloch G (1997) *Initialization of one hidden layer feedforward neural networks for non-linear system identification* 4: 295–300.

Zadrozny B, Elkan C (2001) Learning and making decisions when costs and probabilities are both unknown. In *Proceedings of the Seventh ACM SIGKDD International Conference on Knowledge Discovery and Data Mining*, 204–213.

Zadrozny B, Langford J, Abe N (2003) Cost-sensitive learning by cost-proportionate example weighting. In *Third IEEE International Conference on Data Mining*, 435–442.

Athens Journal of Sciences- Volume 11, Issue 4, December 2024 – Pages 233-260

Uncertainty Analysis in Ecological Risk Assessment: Sensitivity Analysis of Different Exposure Models

By Paul Bovitz[*]

Ecological risk assessments are used for decision making regarding releasing new products to market as well as remedial action required to address contamination at legacy sites. Uncertainty analysis is considered a key part of the process (USEPA 1997) but assessments seldom address uncertainty quantitatively. Key sources of uncertainty include: Sampling and analytical variability (soil/ sediment matrix, lab error), Choice of "Indicator" Species as Target Receptors for Different Exposure Pathways, Sample size. Bioaccumulation and Food Chain Modeling involve assumptions and uncertainty including: Linear assumption of bioaccumulation and selection of bioaccumulation factors; Other model inputs such as: Home range size, Dietary percentages, Body Weights, Ingestion Rate; Literature data on effects, Use of No Observed Adverse Effects Level (NOAEL) or Lowest Observed Adverse Effects Level (LOAEL) as a decision point. Toxicity testing where employed brings its own set of assumptions and interpretation that are subject to uncertainty. These include: Use of single organism, Correlation (or lack thereof) with Contaminants of Concern, Contaminant mixtures, and Reference area selection.

Keywords: *Ecotoxicology, Risk Assessment, Ecology*

Introduction

Another source of uncertainty affecting both food chain modeling and toxicity testing concerns whether the calculated risks and decisions made about them are based on individual or population impacts.

While all of these sources may be important in evaluating potential ecological risks, this paper focuses on the variability and resultant uncertainty associated with food chain modeling results used to predict risks from bioaccumulation. Food chain modeling is often used as the basis for derivation of site-specific remediation goals and hence is an important part of the ecological risk assessment and risk management process at legacy sites. The variability associated with food chain modeling inputs was assessed using test runs of different modeling scenarios to quantitatively evaluate results and conclusions drawn from them. Results and conclusions drawn from ecological risk assessments may vary widely depending on the choice of assumptions, degree of variability and whether or not site-specific empirical data are used as part of the assessment.

This paper focuses on one of the primary measures used to calculate ecological risks at hazardous waste sites in the United States, following USEPA (1997) guidance: food chain modeling. While ecological risk assessment studies may examine a variety of endpoints, this method is perhaps most used for development of remediation goals at contaminated sites for chemical waste products in soil and sediment.

[*]Senior Project Manager, Kleinfelder Inc. (Engineering Company), USA.

Food Chain Modeling Uncertainty

Food chain models typically used in the U.S. for assessment of ecological risks at legacy sites were used as a basis for examining the influence of different model inputs used to calculate risks.

Two target indicator species commonly used in aquatic and terrestrial ecological risk assessments in the U.S. were used as the basis for this study. The aquatic indicator species was the spotted sandpiper (*Actitis macularius*), a migratory shorebird species considered to be the most widespread sandpiper in North America (Cornell Lab 2024). This species is indicative of the sediment and surface water to benthos pathway, as the majority of its food items consist of aquatic and terrestrial insects (Bent 1929).

The terrestrial indicator species chosen was the American robin (*Turdus migratorius*), which is found over much of North America and is a common resident of yards and parklands (Cornell Lab 2024). It feeds primarily on soil dwelling invertebrates such as earthworms during summer months, while in the fall and winter it feeds mainly on fruit (Wheelwright 1986, 1988).

Food chain modeling compares the dose to toxicological effects or toxicity reference values (TRVs) and is expressed by the following formula (USEPA 1997):

$$HQ = \frac{\text{Dose}}{\text{TRV}}$$

Where:

HQ	=	Hazard Quotient
Dose	=	Exposure Point Concentration X Ingestion Rate / Body Weight
TRV	=	Toxicity Reference Value

The dose represents the intake rate of a contaminant, expressed as mg/kg body weight per day. This is a function of the daily food ingestion rate for the target receptor being modeled, the amount of the COPEC in the soil present in the food item (represented by tissue results) and the incidental ingestion of soil.

The full equation for a single exposure pathway (e.g., soil to soil invertebrate to American robin) is given by **Equation 1** (adapted from NJDEP 2024):

$$HQ = \frac{\left(\frac{\left(EPC\ Soil\ \left(\frac{mg}{kg}\right) * BAF * IR\ \left(\frac{kg}{day}\right) * AUF\right) + \left(ISIR\ \left(\frac{kg}{day}\right) * EPC\ Soil\ \left(\frac{mg}{kg}\right)\right)}{BW\ (kg)}\right)}{TRV\ \left(\frac{mg}{kg}\ BW/day\right)}$$

Where:
EPC is exposure point concentration in soil (mg/kg);
BAF is bioaccumulation factor of the contaminant (proportion available for uptake, unitless);
IR is the ingestion rate of the animals (kg food ingested per day);
AUF is the area use factor (unitless; it is the home range in acres divided by the IAOC acres);

The hazard quotient (HQ) is calculated by dividing the dose by a toxicity reference value (TRV), often taken from the literature, and often from a similar species but not necessarily from the exact indicator species being modeled. This is because wild species are much less often tested for toxicity than domestic species or those easily raised for use in laboratory tests. A hazard quotient greater than 1 is indicative of risk.

Typically risk estimates from food chain modeling are calculated using spreadsheets that summarize various assumptions as inputs. The inputs used for ingestion rate (IR), body weight (BW) and Area Use Factor (AUF) are generally taken from literature sources that in the U.S. are standardized (e.g. USEPA Exposure Factors Handbook, 1993). There is some uncertainty associated with the use of those values, in that obviously body weights vary by individual as do home range sizes and even ingestion rates. But in this case standardization of inputs is designed to obtain consistent population level estimates between investigations that apply to "average individuals" not effects as the organism level.

Exposure Point Concentrations (EPCs), Bioaccumulation Factors (BAFs) and Toxicity Reference Values (TRVs) may vary widely, however, and may be site-specific depending on chemical bioavailability. These inputs can greatly affect the assessment of ecological risks and the ultimate decision of whether remediation is required to address site risks.

Selection of Indicator Species

The indicator species chosen to reflect contaminant uptake may be an important determinant of risk calculations. For example, evaluating the soil invertebrate to avian pathway is a pretty standard means of assessing ecological risks. However, some locations (e.g., sandy soil environments) may support very low populations of soil invertebrates, such that modeling this pathway presents a very biased approach in evaluating ecological risks to that community. While this approach was not addressed in this paper, it is worth mentioning as a significant source of uncertainty in risk assessments.

In many cases the species used to evaluate a particular exposure pathway may not be reflective of actual site conditions. For example, while the Spotted sandpiper is often used as an indicator of aquatic risks, it may not be present at a given site, or if, so, only during part of the year. Similarly, habitat variables and quality can be important determinants of whether a species is present. In the case of the Spotted sandpiper shoreline habitats are preferred (Cornell 2024). If a site is thickly vegetated with shrubs for example, the shoreline may not be conducive to their use.

This paper does not go into the differences an investigator may obtain from using different indicator species, but it is worth noting before further discussing species-specific factors affecting the assessment.

Home Range and Area Use Factor Uncertainty

While choosing home range size of an organism would be a straightforward process from the literature, territory and home range sizes may vary seasonally, with

changes in population density, and in areas of different resource quality (Schoener 1968, Sechaud et al. 2022). As a result, home ranges reported in the literature may vary widely for the same species. Often "area use factors" are derived by dividing the site area by the home range to obtain an indication of the amount of time an organism spends at the site. Hence, what home range size is used is key in determining the degree of exposure and hence risks.

In practice the site area is often used as a basis of the area used by the organism since it provides "habitat", but in many cases habitat quality may vary greatly depending on the foraging and roosting characteristics of a species. Using the Spotted sandpiper as an example, one might take the area of a pond and divide it by the home range of the animal. One cannot say that a sandpiper would never use open areas of the pond, but in practice a sandpiper would spend most of its time along the shoreline and in shallow water areas so that mapping those would be a more accurate means of assessing risks to that indicator species. However, that is not usually the case in risk assessments that rely on conservative assumptions.

Methods

Sensitivity Analysis

To quantitatively evaluate the uncertainty associated with three major inputs (EPCs, BAFs, and TRVs), two typical ecological receptors were used. The first was the Spotted sandpiper (*Actitis macularius*), a widespread species representative of many wetland habitats in the U.S. and indicative of the sediment to benthic invertebrates to shorebird exposure pathway. The second was the American robin (*Turdus migratorius*), a common and widely distributed member of the thrush family that feeds largely on soil invertebrates throughout its breeding season (Wheelwright 1988).

To investigate the degree to which different assumptions may affect modeling results, different food chain modeling scenarios were evaluated, as summarized in Table 1.

Table 1. *Food Chain Modeling Inputs Manipulated as Part of the Sensitivity Analysis*

Parameter	Contaminants in Sediment and Soil	Indicator Species	Variables
Exposure Point Concentration (mg/kg of contaminant in soil or sediment)	High molecular weight (HMW) Polycyclic Aromatic Hydrocarbons (PAHs) 4,4'-DDD 4,4'-DDE Copper Lead Mercury Methyl Mercury	Spotted sandpiper (aquatic); American robin (terrestrial)	Mean soil or sediment concentration; 95% Upper Confidence Level (UCL) in Soil or Sediment
Toxicity Reference Values (TRVs)	High molecular weight (HMW) Polycyclic	Spotted sandpiper (aquatic);	Tier 1 TRV (NOAEL)[(1)]

(mg/kg BW/day per contaminant)	Aromatic Hydrocarbons (PAHs) 4,4'-DDD 4,4'-DDE Copper Lead Mercury Methyl Mercury	American robin (terrestrial)	Tier 2 TRV (NOAEL) Tier 3 TRV (LOAEL)[2]
Bioaccumulation Factor (BAF)	Lead	Soil to Earthworms (for use in calculating risks to American robins)	Low BAF (site-specific tissue concentrations used directly); Medium BAF (from literature) High BAF (from literature)
Home Range/Area Use Factor	High molecular weight (HMW) Polycyclic Aromatic Hydrocarbons (PAHs) 4,4'-DDD 4,4'-DDE Copper Lead Mercury Methyl Mercury Zinc (sediment only)	Spotted sandpiper	Territory size (0.25 acre); 3 different Home Range estimates from the literature on breeding density

Sensitivity Analysis of Exposure Point Concentrations

Exposure Point Concentrations (EPCs)

Exposure points concentrations (the amount of a contaminant to which a receptor is exposed) vary based on the number and distribution of samples collected. As a result, uncertainty may be very high in cases where the number of samples collected is low relative to the area under consideration. Uncertainty is also a function of the variability in the soil or sediment matrix (e.g., grain size), as well as contaminant properties (e.g., propensity to adhere to organic carbon, lipid molecules, or volatilization near the surface). Risk calculations may be highly influenced by outliers, or "hotspot" locations since contaminant data is seldom normally distributed. In addition, the calculation of means or 95% upper confidence intervals that are often used as EPCs is affected by the presence of "non-detect" values, in which censored data (such as one half the detection limit) are often used. These values thus may have questionable statistical distributions since the variance is artificially constrained.

Typically risk assessments that rely on data with a high degree of variance have high uncertainty.

Exposure point concentrations were taken from a contaminated site in New Jersey, USA, as a generic example.

Table 2. *Contaminant Concentrations in Surficial (0-6 ") Sediment at 1.08 Acre New Jersey Pond Site. (Shaded Chemicals Were Evaluated Using Food Chain Modeling)*

Chemical	NJ Fresh Water Sediment Lowest Effects Level[1] (mg/kg)	Frequency of LEL Exceedance[7]			Maximum Value[9]	Mean[10] (w/ 1/2 NDs values)
Semi-Volatile Organic Compounds						
1,2-dichlorobenzene	0.294	0	/	33	0.084 U	N/A
1,3-dichlorobenzene	1.315	0	/	33	0.086 U	N/A
1,4-dichlorobenzene	0.318	0	/	33	0.097 U	N/A
1,2,4-trichlorobenzene	5.062	0	/	33	0.089 U	N/A
acenaphthene	0.00671	3	/	33	0.057	0.02
acenaphthylene	0.00587	7	/	33	0.24	0.04
anthracene	0.0572	15	/	33	0.81	0.11
benzo[a]anthracene	0.108	5	/	33	0.35	0.09
benzo[a]pyrene	0.15	2	/	33	0.22	0.08
benzo[b]fluoranthene	10.4	0	/	33	0.49	0.15
benzo[g,h,i]perylene	0.17	12	/	33	0.96	0.21
benzo[k]fluoranthene	0.24	0	/	33	0.23	0.06
chrysene	0.166	15	/	33	1.6	0.26
dibenz[a,h]anthracene	0.033	10	/	33	0.41	0.06
fluoranthene	0.423	1	/	33	0.51	0.12
fluorene	0.0774	3	/	33	0.16	0.04
indeno[1,2,3-c,d]pyrene	0.2	3	/	33	0.35	0.11
naphthalene	0.176	5	/	33	0.82	0.15
phenanthrene	NC	0	/	33	0.75	0.14
pyrene	0.195	7	/	33	0.83	0.19
2-methylnaphthalene	0.0202	15	/	33	1.1	0.18
Low Molecular Weight PAH's with non-detects[3]	NC	0	/	33	2.69	0.64
High Molecular Weight PAH's with non-detects[4]	NC	0	/	33	3.555	0.81
Total Extractable Petroleum Hydrocarbons	NC	0	/	33	15000	2081
Pesticides						
aldrin	0.002	0	/	33	0.47 U	N/A

alpha-bhc	0.006	0	/	33	0.0058	0.04
alpha-chlordane	NC	0	/	33	0.019	0.04
beta-bhc	0.005	2	/	33	0.016	0.18
beta-chlordane	NC	0	/	33	0.69 U	N/A
4,4-DDD	0.00488	25	/	33	27	5.17
4,4-DDE	0.00316	21	/	33	2.9	0.62
4,4-DDT	0.00416	2	/	33	0.016	0.17
delta-bhc	NC	0	/	33	0.012	0.1
dieldrin	0.0019	0	/	33	0.91 U	N/A
endosulfan I	NC	0	/	33	0.61 U	N/A
endosulfan II	NC	0	/	33	3 U	N/A
endosulfan sulfate	0.0346	1	/	33	0.71	0.1
endrin	0.00222	0	/	33	1.9 U	N/A
endrin aldehyde	0.48	0	/	33	0.0054	0.08
endrin ketone	NC	0	/	33	1.7 U	N/A
gamma-BHC	0.003	1	/	33	0.0057	0.05
heptachlor	0.0006	2	/	33	0.0035	0.07
heptachlor epoxide	0.00247	2	/	33	0.041	0.04
methoxychlor	0.0136	0	/	33	5 U	N/A
toxaphene	0.000077	0	/	33	39 U	N/A
Metals and Inorganics						
aluminum	25500	4	/	33	30100	21288
antimony	NC	0	/	33	7.74	4.33
arsenic	6	25	/	33	85.1	45.85
barium	NC	0	/	33	903	506
beryllium	NC	0	/	33	1.4	0.96
cadmium	0.6	25	/	33	12.9	4.74
calcium	NC	0	/	33	63600	23525
chromium	26	25	/	33	192	91.01
chromium VI	NC	0	/	33	43.5 U	N/A
cobalt	50	0	/	33	15.7	10.55
copper	16	25	/	33	376	213
iron	NC	0	/	33	64500	42988
lead	31	25	/	33	4200	1959
magnesium	NC	0	/	33	7870	5548
manganese	630	3	/	33	841	436
mercury	0.174	35	/	36	8.1	4.43
methyl mercury	NC	0	/	33	0.016	0.01
molybdenum	NC	0	/	33	8	6.5
nickel	16	25	/	33	58.2	41.35

potassium	NC	0	/	33	5110	3824
selenium	NC	0	/	33	7.53	3.81
silver	0.5	23	/	33	7.6	4.09
sodium	NC	0	/	33	3030	879
vanadium	NC	0	/	33	212	139
zinc	120	25	/	33	886	417
thallium	NC	0	/	33	4.67	2.4
cyanide (total)	0.1	8	/	33	21	1.74
extractable cyanide	NC	0	/	33	3 U	N/A

Notes: High Molecular Weight PAH's with non-detects calculated as a sum of fluoranthene, pyrene, benz(a)anthracene, chrysene, benzo(a)pyrene, dibenz(a,h) anthracene as provided in http://ceqg-rcqe.ccme.ca/download/en/243, Canadian Sediment Quality Guidelines for the Protection of Aquatic Life.
Half of MDL used for non-detected values. PAH's with non-detects calculated as a sum with non-detects as 1/2 of the MDL. N/A = Not Analyzed. NC = No Criteria Available. mg/kg = Milligrams per kilogram

Table 3. *Contaminant Concentrations in Surficial Soil (0-6 ") at New Jersey Site*

Chemical	**NJ ECO SOIL SSL (mg/kg)**	**Frequency of NJ ECO SOIL SSL Exceedance**			**Mean Value (w/ 1/2 NDs)**	**Maximum Value[9]**
acetone	NC	0	/	139	0.16	1.4
benzene	0.255	0	/	139	0.01	0.083
bromochloromethane	NC	0	/	139	N/A	0.13 U
bromodichloromethane	0.54	0	/	139	N/A	0.13 U
bromoform	15.9	0	/	139	N/A	0.13 U
bromomethane	0.235	0	/	139	N/A	0.25 U
2-butanone	NC	0	/	139	0.02	0.075
carbon disulfide	NC	0	/	139	0	0.033
carbon tetrachloride	2.98	0	/	139	N/A	0.13 U
chlorobenzene	13.1	0	/	139	0	0.004
chloroethane	NC	0	/	139	N/A	0.25 U
chloroform	1.19	0	/	139	0	0.004
chloromethane	NC	0	/	139	N/A	0.25 U
cyclohexane	NC	0	/	139	0	0.028
1,2-dibromoethane	NC	0	/	139	N/A	0.13 U
1,2-dibromo-3-chloropropane	NC	0	/	139	N/A	0.25 U
dibromochloromethane	2.05	0	/	139	N/A	0.13 U
1,2-dichlorobenzene	2.96	0	/	139	0	0.001
dichlorodifluoromethane	NC	0	/	139	N/A	0.25 U

1,2-dichloroethane	21.2	0	/	139	0	0.004
1,3-dichlorobenzene	37.7	0	/	139	N/A	0.13 U
1,4-dichlorobenzene	0.546	0	/	139	N/A	0.13 U
1,1-dichloroethane	NC	0	/	139	N/A	0.13 U
1,1-dichloroethylene	8.28	0	/	139	N/A	0.13 U
cis-1,2-dichloroethylene	NC	0	/	139	N/A	0.13 U
1,2-dichloropropane	32.7	0	/	139	N/A	0.13 U
cis-1,3-dichloropropene	NC	0	/	139	N/A	0.13 U
ethylbenzene	5.16	0	/	139	0	0.024
2-hexanone	NC	0	/	139	N/A	0.38 U
isopropylbenzene	NC	0	/	139	0	0.035
methyl acetate	NC	0	/	139	0.04	2.6
methyl cyclohexane	NC	0	/	139	0	0.079
4-methyl-2-pentanone	NC	0	/	139	0.01	0.013
methyl tert-butyl ether	NC	0	/	139	N/A	0.063 U
methylene chloride	4.05	0	/	139	N/A	0.25 U
styrene	4.69	0	/	139	N/A	0.13 U
tetrachloroethylene	9.92	0	/	139	N/A	0.13 U
toluene	200	0	/	139	0.01	0.37
1,2,3-trichlorobenzene	20	0	/	139	N/A	0.13 U
1,2,4-trichlorobenzene	20	0	/	139	N/A	0.13 U
1,1,2,2-tetrachloroethane	0.127	0	/	139	N/A	0.13 U
1,1,1-trichloroethane	29.8	0	/	139	N/A	0.13 U
1,1,2-trichloroethane	28.6	0	/	139	N/A	0.13 U
trichloroethylene	12.4	0	/	139	N/A	0.13 U
1,1,2-trichloro-1,2,2-trifluoroethane	NC	0	/	139	N/A	0.25 U
trichlorofluoromethane	NC	0	/	139	N/A	0.25 U
trans-1,2-dichloroethylene	0.784	0	/	139	N/A	0.13 U
trans-1,3-dichloropropene	NC	0	/	139	N/A	0.13 U
vinyl chloride	0.646	0	/	139	N/A	0.13 U
m/p-xylene	NC	0	/	139	0.01	0.46
o-xylene	NC	0	/	139	0	0.13
acenaphthene	20	0	/	159	0.03	0.63
acenaphthylene	682	0	/	159	0.03	0.21
anthracene	1480	0	/	159	0.1	1.9
benzo[a]anthracene	5.21	1	/	159	0.3	20
benzo[a]pyrene	1.52	3	/	159	0.27	16

benzo[b]fluoranthene	59.8	0	/	159	0.36	23
benzo[g,h,i]perylene	119	0	/	159	0.27	9.3
benzo[k]fluoranthene	148	0	/	159	0.14	10
chrysene	4.73	1	/	159	0.34	20
dibenz[a,h]anthracene	18.4	0	/	159	0.07	2.4
fluoranthene	122	0	/	159	0.48	35
fluorene	122	0	/	159	0.03	0.38
indeno[1,2,3-c,d]pyrene	109	0	/	159	0.17	8.3
naphthalene	0.0994	83	/	159	0.17	1.1
phenanthrene	45.7	0	/	159	0.35	6.2
pyrene	78.5	0	/	159	0.55	35
1-methylnaphthalene	NC	0	/	139	0.15	0.99
2-methylnaphthalene	3.24	0	/	155	0.27	1.6
Low Molecular Weight PAH's with non-detects	NC	0	/	159	0.95	8.85
High Molecular Weight PAH's with non-detects	NC	0	/	159	2.02	128
Total Extractable Petroleum Hydrocarbons	NC	0	/	136	206	1800
aldrin	0.00332	0	/	141	N/A	0.049 U
alpha-bhc	0.0994	0	/	141	0	0.014
alpha-chlordane	0.224	0	/	141	0	0.014
beta-bhc	0.00398	1	/	141	0	0.01
beta-chlordane	0.224	0	/	141	0	0.012
4,4-DDD	0.758	2	/	141	0.08	7.2
delta-bhc	NC	0	/	141	0	0.019
dieldrin	0.00238	20	/	141	0	0.078
endosulfan I	NC	0	/	141	0	0.0073
endosulfan II	NC	0	/	141	0	0.023
endosulfan sulfate	0.0358	0	/	141	0	0.019
endrin	0.0101	1	/	141	0	0.018
endrin aldehyde	0.0105	14	/	141	0.01	0.11
endrin ketone	NC	0	/	141	0.01	0.14
gamma-BHC	0.005	1	/	141	0	0.0086
heptachlor	0.00598	14	/	141	0	0.021
heptachlor epoxide	0.152	0	/	141	0	0.025
methoxychlor	0.0199	2	/	141	0.02	0.27
toxaphene	0.119	0	/	141	N/A	4 U
aluminum	50	155	/	155	11079	31100
antimony	0.27	130	/	155	1.4	14.3
arsenic	9.9	49	/	160	9.77	64

barium	283	50	/	155	313	2210
beryllium	10	2	/	155	1.08	11.1
cadmium	0.36	92	/	155	0.84	6.58
calcium	NC	0	/	155	88830	376000
chromium	0.4	154	/	155	27.58	110
chromium VI	130	0	/	11	N/A	25.7 U
cobalt	0.14	146	/	155	8.63	34.9
copper	5.4	146	/	155	77.68	408
iron	NC	0	/	155	18496	73500
lead	0.0537	158	/	158	282	2900
magnesium	NC	0	/	155	3618	14900
manganese	220	79	/	155	225	599
mercury	0.1	153	/	176	2.28	31.7
methyl mercury	NC	0	/	20	0	0.0053
molybdenum	2	52	/	139	2.61	19.3
nickel	13.6	113	/	155	32.96	198
potassium	NC	0	/	155	1838	4980
selenium	0.0276	64	/	155	1.88	9.03
silver	1.04	46	/	155	0.93	5.94
sodium	NC	0	/	155	390	7130
vanadium	2	152	/	155	40.11	165
zinc	6.62	143	/	155	231	1770
thallium	1	3	/	155	0.23	3.01
cyanide (total)	1.33	47	/	123	9.29	120
extractable cyanide	NC	0	/	16	N/A	1.1 U

Models were run for both indicator species using the mean, and 95% upper confidence interval (UCL) values for both sediment (Spotted sandpiper) and soil (American robin) and resulting from samples collected at the site. In addition, effects of "outlier" values on the exposure point concentration were evaluated by eliminating those points and rerunning the model.

The exposure points concentrations for different contaminants evaluated in soil and sediment are included in the results tables.

Sensitivity of Toxicity Reference Values (TRVs)

Given their direct influence on the Hazard Quotient calculation, representing the denominator in Equation 1, the choice of TRVs used in modeling has a major impact on the risk estimate calculated. In many cases TRVs are unavailable for the species being modeled at the site. For example, in the case of modeling impacts to the Spotted sandpiper, there may well be no effects data in the literature for a given

contaminant. In such cases, related studies using data from the most taxonomically related species are often used. USEPA will often apply an adjustment factor by dividing the TRV by 10 to account for the uncertainty associated with assuming similar effects to species that are not directly related taxonomically. By attempting to manage uncertainty in this way, it drives risk estimates much higher, and there is no scientific basis for the factor of 10.

USEPA (SSL document) performed comprehensive literature reviews of TRVs for use in developing screening levels for conservative assessment of ecological risks in soil. This approach enables investigators to reduce the uncertainty of risk estimates by focusing on peer-reviewed papers that emphasize effects with known impacts at the population level, such as mortality, reproductive effects, and effects on growth.

However, while the use of the more conservative TRVs are suitable for screening level assessments, review of these documents indicates tremendous variability (often orders of magnitude) in ecotoxicological effects both in studies of the same receptor as well as between receptor species.

Different toxicity reference values taken from the literature were used for comparison of risk estimates to both the Spotted sandpiper and American robin using sediment and soil data from the example New Jersey site. Tier 1 values were taken from the New Jersey Ecological Evaluation Technical Guidance document (2024) and represent conservative No Observable Adverse Effects (NOAEL) values from the literature. In some cases they reflect species data such as mink that are more sensitive than other species regarding contaminant effects. Tier 2 data are also NOAEL data but reflect values used for development of conservative soil screening values (SSLs) used for screening purposes. So while in many cases these are higher numbers than the Tier 1 values, they are still very conservative and tend to overestimate actual risks. Tier 3 values were selected from the literature, usually the same literature used for development of EPA SSL documents, but are focused on survival, growth and reproduction endpoints to receptors most closely related taxonomically to the Spotted sandpiper and American robin. Hence, generally they are less conservative and more realistic indicators of risk than the Tier 1 or 2 values. The sensitivity analysis was conducted using the 95% UCL of the mean sediment and soil values to which the Spotted sandpiper and American robin, respectively would be exposed at the site.

Sensitivity Analysis of Bioaccumulation Estimates

The terms bioaccumulation factor (BAF) and bioconcentration factor (BCF) are often used interchangeably in the literature, but the latter refers primarily to uptake of contaminants by aquatic organisms directly from the water column. Bioaccumulation Factors in food chain modeling are often single values used to represent the proportion of a contaminant expected to be taken up by a given organism, generally a prey item, that is ingested by the receptor being modeled for risk. In reality, bioaccumulation often follows a curve that plateaus at some point where the organism either dies, or becomes sick and avoids the food item it is

ingesting. Differences in BAFs used in modeling can contribute a high degree to the uncertainty of the modeling results.

Bioaccumulation factors were investigated using a single contaminant, lead, as an example of the terrestrial pathway. Site-specific empirical data on earthworm tissue concentrations were used for the food chain modeling. These were derived from a 28-day laboratory investigation of bioaccumulation using "red worms" *Eisenia foetida*, a commonly used earthworm species in laboratory testing and bioaccumulation studies.

Table 4. *Comparison of Soil Concentrations of Various Contaminants of Concern to Earthworm Concentrations Measured in Tissue at the End of a 28-day Laboratory Test*

ANALYTE	Soil Concentration Maximum (mg/kg DW) n = 26	Soil Concentration Mean (mg/kg DW) n = 26	Earthworm Tissue Concentration Maximum (mg/kg DW) n = 0-14	Earthworm Tissue Concentration Mean (mg/kg DW) n = 0-14	BAF based on Maximum Concentration	BAF based on Mean Concentration
SEMI-VOLATILE ORGANIC COMPOUNDS						
benzo[a]anthracene	20	0.31	0.04	0.033	0.002	0.11
benzo[a]pyrene	16	0.29	0.016	0.0063	0.001	0.022
chrysene	20	0.37	0.15	0.071	0.0073	0.19
naphthalene	1.1	0.18	0.0079	0.0073	0.0071	0.04
PESTICIDES						
4,4-DDD	4.9	0.33	0.96	0.092	0.19	0.27
4,4-DDE	0.94	0.047	0.1	0.022	0.1	0.47
4,4-DDT	1.4	0.063	0.045	0.007	0.032	0.11
dieldrin	0.2	0.013	0.004	0.0017	0.02	0.13
endrin aldehyde	0.2	0.018	0.015	0.0015	0.074	0.083
heptachlor	0.07	0.0081	0.0001	0.000095	0.0014	0.012
METALS AND ORGANICS						
arsenic	64	10	3.9	1	0.061	0.097
barium	2210	310	5.1	2.6	0.0023	0.0085
beryllium	11.1	1.1	0.021	0.016	0.0019	0.015
cadmium	14	0.9	2.3	0.63	0.17	0.67
copper	408	78	8.4	4.1	0.02	0.052
lead	1700	275	35.4	4.9	0.021	0.018
mercury	32	2.2	0.34	0.16	0.011	0.07
methyl mercury	0.0053	0.002	N/A	N/A	NC	NC
nickel	198	33	1.4	0.56	0.0072	0.017
selenium	9	3.4	1.1	0.8	0.12	0.24

silver	5.9	1.32	0.086	0.027	0.014	0.02
vanadium	165	41	0.71	0.35	0.0043	0.0086
zinc	1770	229	24.5	17.5	0.014	0.076
Notes:						
mg/kg = milligrams/kilogram						
DW = Dry weight						
BAF = Bioaccumulation Factor derived from data (tissue concentration dry weight/soil concentration dry weight)						

The resultant tissue concentrations in the worms were used to calculate a 95% upper confidence interval (UCL) used for modeling uptake of lead. The BAF was compared to literature-based data on bioaccumulation factors, which vary widely, to investigate the degree of uncertainty involved in typical risk assessments. Different chemicals will have different uptake kinetics, and hence their ability to bioaccumulate will vary. But even using a single contaminant such as lead can illustrate how variable results are on risk assessment findings.

Toxicity reference values were all taken from the literature and include both the No Observable Adverse Effects Level (NOAEL), the concentration below which adverse effects are not seen, and Lowest Observable Adverse Effects Level (LOAEL), the lowest concentration in the literature at which effects are seen. Variability and uncertainty are introduced when the decision is made regarding what receptor to use, and how conservative a value should be chosen to estimate risks. For example, Tier 1 values used by the State of New Jersey are based on agency consensus reflecting highly conservative effects levels so that risk decisions do not result in remaining ecological risks. Tier 2 values represent U.S. Environmental Protection Agency values used to develop Soil Screening Levels (SSLs) that are conservative values used to protect sites, but in many cases are less conservative than Tier 1 values. Tier 3 values represent more realistic values reflecting potential ecotoxicological effects to receptors more closely related taxonomically to the two indicator species investigated.

Data used for modeling soil and sediment concentrations of selected chemicals were taken from an actual manufacturing site in New Jersey, USA. The contaminants chosen were based on those exceeding ecologically based screening benchmarks (USEPA soil screening levels, and New Jersey Department of Environmental Protection Sediment Criteria).

Literature-based values are often used as a basis for calculating the amount of a contaminant present in the tissue. This leads to significant uncertainty and usually an overestimate of the amount of risks present.

Table 5 provides a summary of literature-based values for bioaccumulation of lead from soil-to-soil invertebrates, in comparison to empirically derived data from a site in New Jersey. There is a considerable literature base on bioavailability and uptake of lead into soil invertebrates, and the intent is not to review it here. The focus is on how the variability in bioaccumulation factors reported can influence an ecological risk assessment.

Table 5. *Comparison of Bioaccumulation Factors in the Literature to Empirically Derived Data from a Site in New Jersey*

Bioaccumulation Factor	Source	Comments
Pb log (worm) = 0.74 log (soil) + 0.05	Neuhauser et al. 1995	Indicates relationship is not linear.
Pb Concentration in worm/Pb Concentration in Soil = $14.45*10^{0.9 \log (\text{Soil Pb})}/10$	ERD, USACE Table 1 (1999)	Indicates relationship is not linear.
0.01 to 22, median =0.23	Oorts et al. (2021)	Reviewed 248 papers of bioaccumulation of lead in earthworms.
3.34 (average of 6 papers), range was 0 to 228. Median value = 0.23	Sample et al. (1999)	Best predictive equation (r^2 of 0.78 was based on soil Pb, soil calcium and pH. The 228 number strongly suggests an outlier, since most values in the literature they cited were less than 1.5.
0.05 to 5	Kavehei (2017)	Figure 5.3 of his thesis reviewed results of 12 papers and presented 4 results from his study based on different forms of lead (PbO, $PbCl_2$, $PbCO_3$, and PbS).
0.018	Site-specific number, NJ	Sample size was 7 composite worm samples each of 10 worms, and compared to soil from which they were exposed. See Table 6.

Three different BAF values were used for comparison of model results.

- A low-range value from the literature based on the empirically derived model presented in Sample et al (1999) which predicts concentrations of lead in earthworm tissue based on the soil lead concentration, soil calcium concentration and pH.
- A mid-range literature value (0.23) based on the median value from the Oorts et al. (2021) paper;
- A high-range value based on the maximum value (5) reported in Kavehei (2017).

Sensitivity Analysis of Home Range Size and Other Inputs

The home range size used for food chain modeling of an indicator species can have an important impact on the model results. For some species, such as the Spotted sandpiper, home ranges have not been well studied outside of breeding colonies, leading to uncertainty in the results. This species may nest solitarily, or in colonies (Cornell 2024). While territory is defined as any defended area (Hinde 1956), home range refers to the 'that area traversed by the individual in its normal activities of food gathering, mating, and caring for the young" (Burt 1943). In

birds that exhibit territorial behavior, territory size often reflects population size and resource availability (Stenger 1958, Brown 1969).

Because territory is considered to be a subset of home range size in most cases, use of data on territory size as an estimate of home range size would result in an overestimate of ecological risks from contaminant exposure. This is because if the chemical were present in a discrete area, the smaller the home range of the indicator species, the greater likelihood that it would receive a larger dose of the contaminant if it were living on or near the site.

In the case of the Spotted sandpiper, the standard EPA reference, the Wildlife Exposure Factors Handbook (1993) lists only an estimated territory size taken from a breeding colony and provides no data on home range sizes. In this paper we present literature sources representing several different home range sizes, some from different geographic locations (Table 6).

Table 6. *Territory and Home Range Sizes of Spotted Sandpipers from the Literature*

Territory or Home Range Size	Reference	Comments
0.25 acres	USEPA Exposure Factors Handbook (1993)	Territory size apparently derived from a breeding colony in Minnesota (reported by Maxson and Oring 1980).
12 acres (mean value)	Miller and Miller 1948	Cited in Maxson and Oring 1980
2.5 acres 4.5 acres 8 acres	Hays 1972	Individually marked female birds from a nesting colony in New York
10 individuals per acre when breeding	Oring et al. 1983	Nesting colony on a small island in Minnesota (average breeding density over 9 years)

The different home range sizes were derived from papers reporting the population densities of nesting birds in colonies in Minnesota, California and New York. These are conservative from the perspective of risk estimation because they do not represent the entire foraging radius of individuals but rather the density of nests presents in the colony.

To estimate potential ecological risks different home range sizes ranging from the 0.25-acre territory size to a 12-acre home range were used as inputs to food chain models for the Spotted sandpiper. The risk assessment example was a 1.08-acre pond present at a New Jersey manufacturing facility. To estimate the extent of the area used by the birds, the area of the pond was divided by the home range to obtain an area use factor (AUF). A separate seasonal use factor was used conservatively to indicate the birds were present only during breeding season.

Results

Sensitivity of Different Exposure Point Concentrations

Tables 7 and 8 present results of the food chain modeling using different exposure point concentrations as measures of risk to the Spotted sandpiper and American robin, respectively.

As can be seen in the results, using the 95% UCL results in a higher risk estimate than that using the mean.

Table 7. *Comparison of Hazard Quotients Calculated with Mean and 95% UCL for American Robins*

Hazard Quotients Calculated with Mean and 95% UCL for American Robin					
COPEC	**Mean Concentration in Site Soil (0-6") (mg/kg-DW) n = 26**	**95% UCL in Site Soil (0-6") (mg/kg-DW) n = 26**	**LOAEL (mg/kg BW-WW day) (k)**	**Mean Hazard Quotient (HQ) (unitless)**	**95% Hazard Quotient (HQ) (unitless)**
HMW PAHs	0.329	0.592	0.48	0.05	0.05
Benzo(a)anthracene	0.313	1.37	0.48	0.02	0.03
Chrysene	0.369	1.13	0.48	0.03	0.04
4,4'-DDD	0.334	0.46	2.27	0.01	0.07
4,4'-DDT	0.0629	0.0862	2.27	0	0
Endrin aldehyde	0.0179	0.0121	0.3	0	0
Arsenic	10.02	13.09	2.24	0.11	0.15
Barium	309.7	351.8	41.7	0.12	0.13
Copper	77.7	99.53	4.7	0.33	0.42
Lead	266.1	303.3	1.9	1.91	2.56
Mercury	2.223	3.496	0.9	0.07	0.1
Methyl mercury	0.00198	0.00273	0.026	0.04	0.05
Nickel	32.63	44.01	8.16	0.09	0.13

Table 8. *Comparison of Hazard Quotients Calculated with Mean and 95% UCL for American Robins*

Hazard Quotients Calculated with Mean and 95% UCL for American Robin					
COPEC	**Mean Concentration in Site Soil (0-6") (mg/kg-DW) n = 26**	**95% UCL in Site Soil (0-6") (mg/kg-DW) n = 26**	**LOAEL (mg/kg BW-WW day) (k)**	**Mean Hazard Quotient (HQ) (unitless)**	**95% Hazard Quotient (HQ) (unitless)**
HMW PAHs	0.329	0.592	0.48	0.05	0.05
Benzo(a)anthracene	0.313	1.37	0.48	0.02	0.03
Chrysene	0.369	1.13	0.48	0.03	0.04
4,4'-DDD	0.334	0.46	2.27	0.01	0.07
4,4'-DDT	0.0629	0.0862	2.27	0	0
Endrin aldehyde	0.0179	0.0121	0.3	0	0
Arsenic	10.02	13.09	2.24	0.11	0.15
Barium	309.7	351.8	41.7	0.12	0.13
Copper	77.7	99.53	4.7	0.33	0.42
Lead	266.1	303.3	1.9	1.91	2.56
Mercury	2.223	3.496	0.9	0.07	0.1
Methyl mercury	0.00198	0.00273	0.026	0.04	0.05
Nickel	32.63	44.01	8.16	0.09	0.13
Vanadium	40.8	48.4	0.688	0.38	0.46

Table 9. *Comparison of Hazard Quotients Calculated with Mean and 95% UCL for Spotted Sandpipers*

COPEC		**Mean Concentration in Site Sediment (0-6") (mg/kg-DW) n=0-36**	**95% UCL in Site Sediment (0-6") (mg/kg-DW) n=0-36**	**LOAEL (mg/kg WW-BW day) (l)**	**Hazard Quotient (HQ) (unitless)**	**Hazard Quotient (HQ) (unitless)**
HMW PAHs		1.081	1.555	0.48	0.03	0.04
2-Methylnaphthalene		0.256	0.29	6.7	0	0
Acenaphthene		0.043	0.043	6.7	0	0
Acenaphthylene		0.0848	0.0848	6.7	0	0
Anthracene		0.143	0.22	6.7	0	0
Benzo(a)anthracene		0.103	0.122	0.48	0	0
Benzo(a)pyrene		0.109	0.139	0.48	0	0
Benzo(g,h,i)perylene		0.231	0.303	0.48	0.01	0.01
Chrysene		0.307	0.491	0.48	0.01	0.01
Dibenz(a,h)anthracene		0.111	0.131	0.48	0	0
Fluoranthene		0.141	0.218	0.48	0	0.01
Fluorene		0.04	0.04	6.7	0	0
Indeno(1,2,3-c,d)pyrene		0.127	0.128	0.48	0	0

Naphthalene		0.245	0.286	6.7	0	0
Pyrene		0.31	0.454	0.48	0.01	0.01
4,4'-DDD		5.431	9.305	0.027	28.5	45.56
4,4'-DDE		0.764	1.103	0.027	1.5	1.67
Arsenic		47.89	54.44	3.55	0.22	0.25
Barium		505.52	554.5	41.7	0.12	0.13
Cadmium		5.393	6.444	1.47	0.14	0.16
Chromium		83.15	93.21	2.66	0.44	0.49
Cobalt		10.5524	11.65	7.8	0.07	0.08
Copper		216.5	247.1	4.7	3.73	4.25
Lead		1718	1955	1.9	11.51	13.1
Mercury		3.931	4.374	0.026	9.35	10.39
Methyl mercury		0.0141	0.0251	0.026	0.07	0.1
Nickel		40.48	43.99	6.71	0.19	0.21
Selenium		5.084	5.084	0.29	0.79	0.79
Silver		3.935	4.33	2.02	0.03	0.04
Vanadium		141.9	165.5	0.688	2.01	2.35
Zinc		432.5	492.3	66.1	0.66	0.75

Sensitivity Analysis of Different TRV Values

Table 10 and 11 show the influence of using different TRV values on the estimate of risks to Spotted sandpipers and American robins, respectively. Hazard quotients greater than 1 denote ecological risks.

Table 10. *Sensitivity Analysis of Different TRVs on Risk Estimate for the Spotted Sandpiper*

COPEC	Tier 1 TRV (mg/kg BW day)	HQ	Tier 2 TRV (mg/kg BW day)	HQ	Tier 3 TRV (mg/kg BW day)	HQ
HMW PAHs	0.48	0.035	Not Available	NC	20	0.00084
4,4'-DDD	0.027	46	2.27	0.54	0.028	44
4,4'-DDE	0.027	1.7	2.27	0.020	0.028	1.6
Copper	4.7	4.3	12.1	1.7	61.7	0.32
Lead	1.9	13	3.26	7.6	11.3	2.2
Mercury	0.026	10	Not Available	NC	0.90	0.30
Methyl mercury	0.026	0.10	Not Available	NC	0.064	0.039
Zinc	Not Available	NC	66.1	0.75	131	0.38

Table 11. *Sensitivity Analysis of Different TRVs on Risk Estimate for the American Robin*

COPEC	Tier 1 TRV (mg/kg BW day)	HQ	Tier 2 TRV (mg/kg BW day)	HQ	Tier 3 TRV (mg/kg BW day)	HQ
HMW PAHs	0.48	0.048	Not Available	NC	20	0.0012
4,4'-DDD[1]	2.27	0.065	2.27	0.065	0.028	5.3
4,4'-DDT[1]	2.27	0.0014	2.27	0.0014	0.028	0.11
Copper	4.7	0.42	12.1	0.16	61.7	0.032
Lead	1.9	2.6	3.26	1.5	11.3	0.43
Mercury[2]	0.90	0.10	Not Available	NC	0.9	0.10
Methyl mercury	0.026	0.052	Not Available	NC	0.064	0.021

Table 12 shows the influence of using different bioaccumulation factors (BAFs) on calculated tissue concentrations in earthworm, using lead as an example contaminant of concern, and earthworms as a typical prey item for American robins. These results were compared to the empirical site-specific data obtained from a 28-day bioaccumulation study of soil present on site, measured along a contamination gradient.

Table 12. *Earthworm Tissue Concentrations Measured Empirically versus Estimated by a Range of Bioaccumulation Factors*

95% UCL of Lead in Site Soil (0-6") (mg/kg-DW) n = 26	Bioaccumulation Factor (BAF) (Soil to Earthworms)	Estimated Concentration in Earthworms (mg/kg-DW)
303.30	Empirically Measured 95% UCL	9.52
303.30	Empirically Measured Mean	4.9
303.30	0.23 (median of Oorts et al 2021)	70
303.30	5.00 (selected from papers revised by Kavehei 2017)	1516
303.30	Sample et al 1999 Equation	3.71

Sample et al (1999) equation: ln(earthworm)= B0 + B1(ln[soil]) +B2(ln[soil Ca])+ B3(pH)
where B0=intercept, B1=soil coefficient, B2=soil Ca coefficient, and B3= pH coefficient.
B0 = 2.45, B1= 1.18, B2= 0.06, B3= -.93

In the case of American robins, tissue data collected from the site were used to estimate the concentration of contaminants being ingested by the birds. Focusing on lead, approximately 3% of the lead in soil was present in depurated tissue of the earthworms. Site-specific values can provide a much more accurate estimate of the bioavailability of the soil contaminants present, in this case lead. Actual prey item tissue concentrations may be used in place of a bioaccumulation factor to estimate risks. It should be noted that collection of empirical tissue data may be more expensive and involves careful study design to ensure that the entire soil contamination gradient is assessed. Table 13 shows the effect of using different BAFs on risk estimates for the American robin.

Table 13. *Results of Food Chain Modeling for American Robin Based on Different Bioaccumulation Factors*

Bioaccumulation Factor	Earthworm Concentration (95% UCL), Measured or Modeled	Hazard Quotient to American robins
Empirically Measured 95% UCL	9.52	2.56
Empirically Measured Mean	4.9	2.12
Median of Oorts et al (2021) =0.23	70	8.26
Selected from Kavehei 2017 as higher value = 5	1516	145
Sample et al 1999 Equation	3.71	2.01

Results of the analysis indicate that the Sample et al (1999) model came close to predicting the actual earthworm tissue lead concentration if the mean lead concentration (not 95% UCL) value is used. The effect of using the modeled concentration resulted in similar risk estimates for the American robin as the hazard quotients are both near 2.0. Using other literature-based numbers, however, greatly overestimated risks.

Sensitivity Analysis of Home Range Size on Risk Estimates for Spotted Sandpiper

Table 14 provides the results of the food chain modeling with different home range sizes from the literature.

Table 14. *Results of the Sensitivity Analysis of Home Range Size on Hazard Quotients Calculated for Spotted Sandpipers*

COPEC	95% UCL	Area Use Factor[(a)]				Hazard Quotient			
	Concentration in Sediment	0.25 acre	2.5 acre	4.5 acre	12 acre	0.25 acre	2.5 acre	4.5 acre	12 acre
4,4'-DDD	9.305	1	0.432	0.24	0.09	45.56	19.68	10.93	4.1
4,4'-DDE	1.103	1	0.432	0.24	0.09	1.67	0.72	0.4	0.15
Copper	247.1	1	0.432	0.24	0.09	4.25	1.84	1.02	0.38
Lead	1955	1	0.432	0.24	0.09	13.1	5.66	3.14	1.18
Mercury	4.374	1	0.432	0.24	0.09	10.39	4.49	2.49	0.94
Methyl Mercury	0.0251	1	0.432	0.24	0.09	0.1	0.04	0.02	0.01
Zinc	5.084	1	0.432	0.24	0.09	2.35	0.32	0.18	0.07

[(a)]Calculated by taking 1.08-acre Pond Area and dividing by Home Range.

Discussion

Exposure Point Concentrations

In the food chain modeling conducted of both the Spotted sandpiper and American robin, use of the 95% UCL as the exposure point concentration gave higher estimates than that of the mean. This is not surprising, given that the 95% UCL is affected by higher values in the distribution, and contaminant data are often lognormally distributed. In some cases these higher values represent "hot spots" that may be addressed by remediation. But there is always considerable uncertainty regarding the exposure point concentration because it is affected by sample size, variability in the soil matrix, and in some cases the spotty nature of contaminant distribution in fill material and other soil substrates affected by atmospheric deposition and other sources. Moreover, analytical data from soil or sediment represent a very small sample volume, as low as 0.5 g of material (USEPA Method SW-846). An individual analytical result is then used to represent the contamination found at a location that may be 10 m in radius or more. Resampling or duplicate samples can provide an indication of the variability associated with sampling results but is expensive and typically quality assurance and control procedures are based on 1 out of 10 samples being duplicated. The variability can be substantial and significantly affect risk estimates.

Consider the following table of results obtained when conducting the earthworm bioaccumulation study cited above.

Table 15. *Comparison of Maximum Analytical Data Originally Selected for Testing versus Concentrations Detected in Actual Soil Samples Used for the Earthworm Bioaccumulation Study*

Analyte	**Location**	**Prior Maximum Concentration (Jan 2018)**	**Resampled Concentration (Oct-Dec 2018)**
Unit		**mg/kg**	**mg/kg**
4,4'-DDD	CSB-645	2.3	0.12J
Toxaphene	CSB-645	98	ND
Arsenic	CSB-647	143	32.4
Barium	CSB-647	5210	121
Chromium	CSB-670	611	76.6
Copper	CSB-666	700	150
Lead	ESB-489	2900	501
Mercury	ESB-520	31	22.8
Vanadium	CSB-546	2090	36.3
Zinc	ESB-447	1770	1500
Cyanide	ESB-514	120	6.6

This paper focused on lead, and review of the maximum concentration intended to be measured indicates when the same location was resampled a few months later, a much lower concentration was detected. This cannot be explained by attenuation or any other natural process, but rather reflects the random variability associated with sampling a second time at the same depth. This phenomenon was not confined to lead concentrations; while some parameters such as zinc showed similar results between events, many others such as 4,4'-DDD, arsenic, barium, chromium, and copper were detected at significantly lower values during the second event. This variability is significant, and the earthworm study were not conducted, and the original soil data were used along with literature-based bioaccumulation factors, a significantly higher risk estimate would have resulted.

Analytical methods can also affect results and may have been a factor in the above results. Typically, analytical methods such as EPA SW-846 of metals require reproducibility of matrix spikes to fall within 20% of the known matrix spike in order for results to meet QA/QC criteria (USEPA 2024). With respect to organics, the criterion is often 30%. With such variability in analytical results, risk estimates could vary significantly as a result of analytical testing alone. If analytical variability and sampling variability are both accounted for, the resulting variability could result in order of magnitude differences in risks calculated to indicator species. Yet risk assessments seldom calculate this range quantitatively.

Toxicity Reference Values

One of the greatest sources of uncertainty in food chain modeling may well be from the choice of TRV in calculating risks. Values are often suggested or required by regulatory agencies to allow conservative decisions to be made regarding whether a legacy site may require remediation. However, in some cases the assessments are made based on singe research papers that are decades old and which have not been repeated experimentally to achieve the same or similar results. Many times, these studies are entirely laboratory based and the measure of effects is based on experimental feeding trials or dosage studies that use highly available forms of contaminants that may not represent the same forms that would be found in nature within sediments or soil. Highly bioavailable forms are used so that researchers can see at what concentrations effects are evident, as opposed to studies of soil or sediment from the field that may show little or no effect.

Yet, conducting food chain modeling based on expensive, carefully measured empirical data collected from the field on sediment, soil and tissue and then using it to calculate a dose that is then compared to a single laboratory-based study is problematic. In-situ field tests in which an organism is exposed to soil or sediment under natural conditions may be a solution, but the organism should be one that would normally occur at the site and acclimated to site conditions. Such tests often fail for not meeting those criteria. For example, exposing earthworms such as *Eisenia foetida* (characteristic to European dung piles) may not be appropriate in evaluating sandy soils contaminated with lead in the U.S. The animals could react

adversely to low pH, grain size or lack of organic matter necessary for food during a 28-day test, for example.

In this current study the choice of TRV clearly affected risk estimates. Although results would still indicate the need for remedial action in some cases if a lower TRV were chosen, the results would be different if a different data set were applied (e.g., at lower soil concentrations of 4,4' DDE to American robins for example.

Bioaccumulation Factors

Risk estimates to American robins were highly influenced by the choice of bioaccumulation factors used to determine the concentration of lead in earthworm tissue. The hazard quotients used to estimate risk varied by over an order of magnitude. These estimates would be even higher if a receptor that fed entirely on earthworms were modeled, such as a shrew, or American woodcock. While it varies seasonally, the American robin's diet is approximately half vegetative material (Wheelwright 1988). If a receptor were modeled that ingested almost exclusively earthworms, these hazard quotients would be nearly twice as high. Moreover, the hazard quotients calculated were based on a site with moderate lead contamination (e.g., approximately 300 mg/kg dry weight on average) in surficial soils, which is much lower than some mining or manufacturing sites where concentrations may be in the thousands of parts per million.

Risk estimates calculated using the literature based BAFs would be even more overestimated if the soil data were higher because of the direct relationship between soil concentration and earthworm concentrations in the model. Lead bioaccumulation is not necessarily linear and hence at higher soil concentrations the amount in tissue would be overestimated by a single BAF.

Several papers have specifically focused on uptake of lead by various species of earthworms in laboratory bioaccumulation tests (Bradham et al. 2006, Sandifer et al. 1996, Kiewet et al. 1991). These, and other investigations cited in Table 5 of this paper indicate a high degree of variability based on soil properties with BAFs ranging from 0.01 to 22.05.

Why would bioaccumulation factors in the literature from soil to earthworms vary so much? The potential factors include:

1. Experimental design.
2. Form of lead present.
3. Soil characteristics affecting bioavailability, including pH, calcium concentrations, organic matter, and grain size.
4. Amount that the worms are depurated.

Bioaccumulation factors cited in the literature that are far greater than 1 are likely an overestimate of the actual amount present in earthworm tissue for a chemical such as lead, which although it can be toxic is not considered a strong bioaccumulator in terrestrial food chains (ATSDR 2007, Eisler 1988). According to Eisler (1988), lead poisoning in higher organisms has been associated with lead

shot and organolead compounds, but not with food chain exposure to inorganic lead in soil (other than direct ingestion of lead shot, sinkers or paint).

Calculated BAFs such as the 228-maximum cited in Sample et al. (1998) appear to be outliers may reflect situations where the earthworms were not fully depurated prior to analysis. Such BAFs should not use in risk assessment modeling. Neither should BAFs that are based on laboratory studies of earthworm uptake by forms of lead that are highly bioavailable, but not often found in nature.

Regardless of whether bioaccumulation is measured in field or laboratory studies, depuration is critical to standardization of results. Why depurate earthworms as a basis for risk estimates? Because the soil fraction is already accounted for in the models, and the soil fraction itself is overestimating risks because it is not 100% bioavailable. In fact, because there is no adjustment in the model for the bioavailability of lead in soil, the soil fraction often drives the estimate of risk. The estimate is biased high because typically only a portion of the lead in soil may be assimilated in a form that is mobilized upward through the food chain. While it is true that birds would consume the soil inside the earthworm and not depurate it first, it is the portion in tissue that is most bioavailable and hence likely to be passed upward through the food chain. Ingestion of soil lead can be mitigated by diets high in protein and calcium which tend to inhibit absorption in the digestive system (reviewed in Franson and Paine 2011, p. 568).

As Sample et al. (1998), site-specific studies of bioaccumulation are nearly always more accurate than literature-based results. Site-specific bioaccumulation may be measured two different ways. In the case of earthworms, the first approach is to collect worms at the site and depurate them. The drawback to this approach is it is limited to where worms are present. Highly contaminated areas or locations with poor soil characteristics (coarse grain size, little organic matter) may not be supporting sufficient worm populations to sample. In addition, it may be difficult to relate the resultant tissue concentrations back to the soil concentration. For example, suppose it takes a meter- squared plot to obtain sufficient biomass to measure tissue concentrations. Establishing a mean soil concentration over such a large area may require several surficial samples to be collected and analyzed. A single composite sample may not reflect concentrations to which the worms are exposed.

A second approach would be to look at existing soil analytical data to determine a sampling gradient. Those locations can be resampled to confirm the gradient and expose the worms to sufficient soil in the laboratory to obtain estimates of uptake over a 28-day period. The actual worm tissue data are then used to calculate risks. If risks are observed, the empirically derived BAFs can be used to back calculate the concentration in soil that is "safe" as a basis for remedial action recommendations. A drawback of this approach is the original contaminant gradient observed may not be reproducible (see Table 12 above for an example. For that reason, it is a good practice in designing such studies to include "extra" or duplicate locations to help ensure that the worms analyzed reflect the range of concentrations present at the site.

Conclusions and Recommendations

This paper has focused on many sources of uncertainty in ecological risk assessments that have been known about for years but are seldom quantified to evaluate their impact on risk estimates. Specifically, food chain modeling relies on several critical assumptions that may significantly affect risk estimates.

These include exposure point concentrations calculated for soil and sediment, literature-based bioaccumulation factors, toxicity reference values from most sensitive species, and home range sizes assessed from limited data. In example calculations from a site in New Jersey the variability in such inputs resulted in differences in risk estimates to the Spotted sandpiper and American robin that sometimes varied over an order of magnitude.

Specific recommendations to improve the reliability of risk estimates used for remedial action decisions included the following.

1. Re-evaluate or replicate older (e.g., decades old) toxicity studies that are still used as a basis for many risk assessments to verify their validity.
2. Conduct more toxicological studies on wildlife species as opposed to common laboratory animals (e.g., rats, mice) that then require extrapolation to wild animals.
3. Avoid applying TRVs that were developed as a basis for screening benchmarks to risk assessments used as a basis for remedial action decisions.
4. Ensure that indicator species modeled inhabit or can inhabit the site, and that AUFs calculated reflect the actual extent that the species could use the site.
5. Regulatory agencies would benefit from developing databases of site-specific studies conducted at legacy sites nationwide for sharing information on risks. This "gray literature" (not peer-reviewed or in journals) could provide very useful information on actual site-specific risks that has not been reported in the literature that is dominated by (often older) laboratory-based toxicity studies.

Implementation of regulatory policies designed to obtain more realistic risk estimates could allow refocusing regulatory efforts, including research and funding toward other initiatives such as habitat preservation via conservation easements, and land acquisition as part of the risk management process. This could result in more positive ecological benefits than remediation of sites that may not actually require it based on overestimates of risks.

References

Bent AC (1929) *Life histories of North American shore birds*. U.S. Natl. Mus. Bull. 146, part 2.

Bradham KD, Dayton EA, Basta NT, Schroder J, Payton M, Lanno R (2006) Effect of soil properties on lead bioavailability and toxicity to earthworms. *Environ. Toxicol. Chem.* 25: 769–775.

Brown JL (1964) The evolution of diversity in avian territorial systems. *Wilson Bull.* 76: 160–169.

Burt WH (1943) Territoriality and home range concepts as applied to mammals. *J. Mammal*. 24: 346–352.

Cornell University, Laboratory of Ornithology (2024). *Birds of the World*. Available at: https://bird softheworld.org/bow/species/sposan/cur/introduction.

Eisler R (1988) *Lead hazards to fish, wildlife, and invertebrates: a synoptic review*. U.S. Fish Wildl. Serv. Biol. Rep. 85(1.14).

Environmental Restoration Division (ERD) Manual (1999) *Bioaccumulation and Bioconcentration Screening Manual: ERD-AG-003*.

Franson J, Paine DJ (2011) Lead in Birds. In N Beyer, JP Meador (eds.), *Environmental Contaminants in Biota: Interpreting Tissue Concentrations*. CRC Press, Boca Raton.

Hays H (1972) Polyandry in the Spotted Sandpiper. *Living Bird* 11: 43–57.

Hinde A (1956) The biological significance of territories in birds. *Ibis* 98: 340–564.

Kavehei A (2017) *Effects of earthworms on leachability of lead in soils*. M.S. thesis, University of Macquaurie, Sydney, Australia.

Kiewet AT, Ma WC (1991) Effect of pH and calcium on lead and cadmium uptake by earthworms in water. Ecotox. *Environ. Safety* 21: 32–37.

Maxson SJ, Oring LW (1980) Breeding season time and energy budgets of the polyandrous spotted sandpiper. *Behaviour* 74: 200–263.

Miller RT, Miller J (1948) Nesting of the Spotted Sandpiper at Detroit, Michigan. *The Auk* 65: 558–567.

Neuhauser EF, Cukic ZV, Malecki MR, Loeher RC (1995) Bioconcentration and biokinetics of heavy metals in the earthworm. *Environmental Pollution* 89: 293–301.

New Jersey Department of Environmental Protection (NJDEP) (2024) *Ecological Evaluation Technical Guidance*.

Ooorts K, Smolders E, Lanno R, Chowdbury MJ (2021) Bioavailability and Ecotoxicity of Lead in Soil: Implications for Setting Ecological Soil Quality Standards. *Environ. Toxicol. Chem.* 40: 1948–1961.

Oring LW, Lank DB, Maxson SJ (1983) Population studies of the polyandrous Spotted Sandpiper. *The Auk* 100: 272–285.

Sample BE, Opresko DM, Suter GW (1998) *Toxicological Benchmarks for Wildlife: 1996 Revision*. Oak Ridge National Laboratory.

Sandifer RD, Hopkin SP (1996) Effects of pH on the Toxicity of Cadmium, Copper, Lead and Zinc to *Folsomia candida* Willem, 1902 (Collembola) In a Standard Laboratory Test System. *Chemosphere* 33(12): 2475–2486.

Schoener TW (1968) Sizes of feeding territories among birds. *Ecology* 49: 123–141.

Sechaud RK, Schalcher K, Almasi B, Bühler R, Safi K, Romano A, et al. (2022) Home range size and habitat quality affect breeding success but not parental investment in barn owl males. *Scientific Reports* 12: 6516.

Stenger J (1958) Food habits and available food of Ovenbirds in relation to territory size. *Auk* 75: 335–346.

Swarth C (1988) *Spotted Sandpiper (Actitis macularius) Species Account in, California Wildlife Habitat Relationships System*. California Department of Fish and Wildlife.

U.S. Department of Energy, Hazardous Waste Remediation Program (HAZWRAP) (1994) *Appendix M - Ecological Risk Assessment*.

U.S. Department of Health and Human Services, Public Health Service, ATSDR (2007) *Toxicological Profile for Lead*.

U.S. Environmental Protection Agency (USEPA) (1993) *Wildlife Exposure Factors Handbook*. EPA/600/R-93/187.

USACE (2019) *Biota-Sediment Accumulation Factors (BSAF database)*. U.S. Army Corps of Engineers.

USEPA (1997) *Ecological Risk Assessment Guidance for Superfund*.

USEPA (2005) *Ecological Soil Screening Level (Eco-SSL) Guidance and Contaminant Specific Documents*. U.S. Environmental Protection Agency Office of Solid Waste and Emergency Response, Washington D.C.

USEPA (2005) *Ecological Soil Screening Levels for Copper*, Interim Final.

USEPA (2024) *Quality Assurance/Quality Control web page for Method SW-846*. https://www.epa.gov/hw-sw846/quality-assurance-qa-quality-control-qc

Wheelwright NT (1988) Seasonal changes in food preferences of American robins in captivity. *Auk* 105: 374–378.

Athens Journal of Sciences- Volume 11, Issue 4, December 2024 – Pages 261-286

A Digital-based Model Proposal for Optimum Building Orientation in Architecture in Ecological Context

By Nur Sumeyye Yalcin Kocak[*], Ibrahim Agah Tastemir[±], Erdem Koymen[°] & Enes Yasa[•]

In order to make optimum use of the heat energy coming from the sun and the cooling effect of the wind, it is very important that the buildings are positioned on the land in positions that can provide the highest level of user comfort with minimum energy consumption. Determining the layout of the building is a critical design parameter that affects energy consumption. However, when there are vistas such as sea, forest, etc. that are desired to be seen from the first degree interior volumes around the building, this factor becomes decisive in the building orientations. As a result of this, climatic comfort factors such as natural ventilation provided by wind and heat energy from the sun are ignored. While the orientation of the interior spaces towards the landscape is preferred by the users, the climate element and the comfort it provides should be the priority in the architectural design. In this study, an orientation optimization model has been proposed for building orientation based on utilizing vista and climatic data in the context of passive design. With the parametric and numerical-based approach developed in the study, the way to use the vista factor, which has a multivariate and complex structure, as an "input data" has been investigated. In order to test and verify the developed optimization model, "The Canal Istanbul" artificial waterway project area, which is a very up-to-date subject, was chosen as the plot research area. The Canal feasibility studies have been prepared by the authorities. The data obtained from these reports were used quantitatively in the model. In this context, the technical and ecological data of the canal route were investigated from the reports prepared for the Canal Istanbul route. Thus, as a result of the data accessed from various sources, the climate type and ecological characteristics of the region have been moved to a quantitative dimension as numerical data. An optimization model has been developed for optimum building orientation in terms of regional climate, taking into account the zoning decisions and basic planning criteria determined in the focus of these data. The developed model primarily places the building in the desired point position over the 1000 and 5000 zoning plans of the region, with the vista as priority. Afterwards, the model perceives the vista spline that enters the field of view of the building. Then, staying within the boundaries of this spline, it turns the structure in alternative directions and analyzes it according to each direction. At this stage, the model presents a mathematical dataset by comparing the alternative orientations of the building with the "optimal direction", "prevailing wind direction" and "north direction" angles. Finally, these data are optimized within the model and suggestions are made to the designer to make a choice, based on the results obtained.

[*]Lecturer, Istanbul Commerce University, Turkey.
[±]Research Assistant, Istanbul Sabahattin Zaim University, Turkey.
[°]Lecturer, Istanbul Sabahattin Zaim University, Turkey.
[•]Associate Professor, Istanbul University, Turkey.

Introduction

The loss of life and property for many years due to ship accidents in the Bosphorus has prompted the authorities to take measures to prevent these accidents. However, despite the measures taken, it is known that ships still pose a danger in the strait. It was decided by the authorities to open an alternative artificial waterway to the Bosphorus, for reasons such as protecting the historical center of Istanbul, ensuring the safety of the Bosphorus and relieving traffic.[1] For this reason, the Canal Istanbul Project, which is planned to be built, has emerged as an artificial waterway project that will connect the Black Sea and the Sea of Marmara in parallel with the Bosphorus by digging the mainland on the north-south axis on the European side of Istanbul. The project area is divided into 7 stages and as of 2022, the zoning plan for 3 stages has been prepared. In this article, a model has been proposed in order to interpret and qualify the vista-oriented building orientation that will occur in the region with Canal Istanbul, with climatic comfort parameters.

As it is known, "comfort" is a very important component to meet human needs. Arrangements made in the artificial environment significantly affect the indoor comfort and cause positive or negative results for the building-indoor occupant. When the decisions taken at the upper scale are sustainable, energy-conserving designs emerge. The location of the building, the distances between the buildings, its form, volume, building elements and orientation are the most important parameters that affect energy conservation. Buildings built by considering these parameters are also described as "clean energy".[2]

Energy consumption is increasing in direct proportion to the increase in industrialization and population in the world, and this causes air pollution, an increase in temperature, and subsequently the melting of glaciers and a rise in the water level. Continuing to use fossil fuels poses a danger to the ecosystem. With the widespread use of renewable energy sources, it may become possible to prevent ecological problems. The use of natural energy resources in building designs based on an energy efficient system and the selection of building components in this direction provide environmental sensitivity.[3]

It can be said that one of the most important parameters leading to climate change is urbanization. Both the most affected and the most affected areas are cities. People who migrated from rural areas to cities for economic, social and political reasons started the unplanned and uncontrolled urbanization process. When the number of people living in cities is examined worldwide since the industrial revolution, a significant increase is observed. While the urban

[1]Kesici, Ö. "İstanbul Boğazı varken neden kanal istanbul?" (Why Canal Istanbul when there is the Bosphorus?) 4. In *Uluslararası Bilimsel Araştırmalar Kongresi* (s. 227-252). Ankara: Sosyal Bilimler, 2019.

[2]Manioğlu, G. "Geleneksel Mimaride İklimle Uyumlu Binalar: Mardin'de Bir Öğrenci Atölyesi." (Climate Compatible Buildings in Traditional Architecture: A Student Workshop in Mardin.) In VIII. Ulusal Tesisat Mühendisliği Kongresi, 79-92. İzmir, Turkey, 2007.

[3]Mangan, S. D. Akıllı binalarda alt sistem değerlendirmesi: İstanbul örneği. (Subsystem evaluation in smart buildings: Istanbul example.) İstanbul: İstanbul Teknik Üniversitesi, Fen Bilimleri Enstitüsü, Mimarlık Anadilim Dalı, Çevre Kontrolü ve Yapı Teknolojisi, 2006

population, which was 14% in the 1900s, increased to 47% in the 2000s, it is predicted that it will be 60% in 2030.[4]

Increasing population brings with it many problems. Insufficient housing areas have led to a decrease in green areas over time. In this context, Odul and Cagdas (2019)[5] investigated whether structural changes have an impact on the climate by considering the Inkilap, Madenler and Site Areas of Umraniye district of Istanbul. Using GIS and Remote Sensing methods, they examined Landsat thermal satellite images of the last 16 years before 2019 and determined that the structural changes in the natural topography changed the climate structure. This study has been taken into consideration in order to discuss whether the construction after the canal construction will give similar results.

High structures or low but close-range structures have a significant share in the warming effect. While the construction of pavements, roads and living spaces instead of vegetation creates more warming in the region, it is thought that the structures or landscaping that are not made according to the climatic characteristics of the region cause meso-micro climate change in the region. It is very important to protect the natural vegetation around the buildings and to increase the green areas in order to reduce the negative effects of unplanned and uncontrolled construction on the temperature. It is possible to prevent the increase in temperature by creating air corridors by constructing structures that do not prevent air currents and making the forms, heights and layouts of the buildings in a planned manner. It is known that the structures built by the sea prevent the sea breezes that serve to clean the air.[6]

The wind parameter also affects the climate and this situation changes according to the topography. When it is desired to take advantage of the cooling effect of the wind; It is very important in terms of climatic comfort that the long facade of the building is oriented according to the prevailing wind direction, and when it is desired to benefit from the radiant heat of the sun, the places where the building will spend the most time are directed towards the south facade. It is necessary to place the areas where the most time is spent during the day, such as the living room, bedrooms and kitchen, which are in the 1st degree volume group, to the south and near the south, and the wet areas such as the bathroom and toilet, which are in the 2nd degree volume group, to be placed according to the other aspects of the building in terms of heat gain. It is necessary to use sunshade elements for sun protection.[7]

---

[4]Çobanyılmaz, P., and Yüksel, Ü. D. "Kentlerin iklim değişikliğinden zarar görebilirliğinin belirlenmesi: Ankara örneği." (Determining the vulnerability of cities to climate change: Ankara example.) Süleyman Demirel Üniversitesi Fen Bilimleri Enstitüsü Dergisi 3, no. 17 (2013): 39-50.

[5]Ödül, H., and Ç. K. Kentsel alanda iklimsel değişimin incelenmesi: Ümraniye örneği. (Examining climatic change in urban areas: Ümraniye example.) Ankara: TMMOB 6. Coğrafi Bilgi Sistemleri Kongresi, 2019.

[6]Şimşek, Ç. K., and B. Şengezer. İstanbul metropoliten alanında kentsel ısınmanın azaltılmasında yeşil alanların önemi. (The importance of green areas in reducing urban warming in the Istanbul metropolitan area.) Megaron 7, no. 2 (2012): 116-128.

[7]Balcıoğlu, A. Geleneksel ve modern bağ evi örneklerinin soğutma enerjisi korunumunda etkili olan tasarım değişkenleri açısından değerlendirilmesi. (Evaluation of traditional and modern vineyard house examples in terms of design variables effective in cooling energy conservation.) İstanbul:

The effect of the distance to be left between the buildings according to the climatic characteristics is also important. The distance is directly proportional to the building heights. In the temperate-humid climate zone, the distance between buildings can be determined at the rate of H-5H in the prevailing wind direction and 2-3H according to the sun (north-south direction).[8] In the literature, it is recommended to use free building forms and cruciform forms in temperate-humid climatic regions. The ratio of building lengths to widths of 1.6 provides optimum comfort effect. While the building form is optimum with a ratio of 1:1.6 on the east-west axis, it is stated that the maximum ratio should be 1:2.4.[9]

The orientation of the building is as important as its shape and form. In their study, Umarogullari and Cihangir (2019)[10] analyzed Edirne Binevler (1st Section) houses located in the temperate-humid climate zone according to the climate-balanced design parameters, and calculated whether 40 building blocks with A, B, C types could meet the optimum value in building orientation, and it was determined that 40% of the 40 blocks could meet the optimum value. He found that 70 of them were not positioned according to proper orientation.

Keskin and Engin (2019)[11] conducted a research in Cukurcayir, a new and dense settlement of Trabzon, which has a temperate-humid feature. In the research, they determined two housing units from the north, east and west directions and examined the distance, orientation and passive system decisions of the buildings for six housing units. In this research, it has been determined that the housing estates are not directed to benefit from or be protected from the sun and wind, and that the decision for an energy efficient passive system is not taken when there is a possibility.

Meric, Manioglu and Aksit (2013)[12] analyzed the multi-storey houses of mass housing projects in Istanbul Maslak, which have the same characteristics but different orientation, in terms of energy. They determined that the effect of 4 houses on the same floor of a building having different orientations on climatic comfort is not only the result of the orientation of the building, but also changes

---

İstanbul Teknik Üniversitesi, Fen Bilimleri Enstitüsü, Mimarlık Anabilim Dalı, Çevre Kontrolü Ve Yapı Teknolojileri Programı, Master's Thesis, 2013

[8]Ovalı, P. K. Biyoklimatik tasarım matrisi (Türkiye*).* (Bioclimatic design matrix (Türkiye).) *Trakya Üniversitesi Mühendislik Bilimleri Dergisi* 20, no. 2 (2019): 51-66.

[9]Ovalı, P. K. *Türkiye iklim bölgeleri bağlamında ekolojik tasarım ölçütleri sistematiğinin oluşturulması "Kayaköy yerleşmesinde örneklenmesi".* (Establishing a systematic of ecological design criteria in the context of Turkey's climate zones "Exampling in Kayaköy settlement".) Edirne: T.C. Trakya Üniversitesi, Fen Bilimleri Enstitüsü, Mimarlık Anabilim Dalı, Doctoral dissertation, 2009

[10]Umaroğulları, F., and C. Cihangir. Toplu konutların iklimsel konfor tasarım parametrelerine göre değerlendirilmesi: "ılıman nemli iklim bölgesi: Edirne binevler (1.kısım) konut yapı kooparetifi örneği. (Evaluation of mass housing according to climatic comfort design parameters: "temperate humid climate zone: Edirne binevler (1st part) housing building cooperative example.) Mimarlık ve Yaşam Dergisi 4, no.1 (2019): 105-122.

[11]Keskin, K., and N. Engin. "Toplu konutlardaki yerleşim kararlarının enerji etkin mimarlıktaki rolü." (The role of layout decisions in mass housing in energy efficient architecture.) Mimarlık ve Yaşam Dergisi 4, no. 1 (2019): 69-78.

[12]Meriç, Z., G. Manioğlu, and Ş. F. Akşit. "Çok katlı konutların enerji korunumu açısından performansının değerlendirilmesi." (Evaluation of the performance of multi-storey houses in terms of energy conservation.) In 11. Ulusal Tesisat Mühendisliği Kongresi, (s. 1447-1456). İzmir, 2013

depending on the form of the building. In his study, Varoglu (2017)[13] examined the optimum orientation and optimum shading in buildings located in hot climate regions and proposed a method for Cyprus, taking into account the total annual energy consumption of the building.

Topcu (2020)[14] examined the Istanbul Kayabasi Mass Housing Example in an ecological context. He stated that the buildings are oriented in accordance with the slope so that they do not block the vista of each other and can benefit from the sun to the maximum, and the buildings are positioned with a slope of 45% in order to reduce the wind speed. According to the information obtained from this study, which is thought to contribute to the article in terms of optimum orientation, it has been seen that shape, form and orientation provide gain in energy consumption by taking into account the climatic comfort parameters.

Turan (2019)[15] gave information about the location of the canal route and the geographical features of the area in his study. In addition, climatic parameters such as precipitation, temperature and wind were evaluated with tables, graphics and maps according to the data obtained from Kumkoy, Yalikoy, Florya, Buyukcekmece, Arnavutkoy and Cerkezkoy stations. This study was used to determine the geographical and climatic parameters of the area.

Aksin (2019)[16] examined the houses with a similar type of design, which are frequently found in Ankara. In research, he made a performance evaluation on the simulation built by Grasshoper3d with Ladybug, Honeybee and Octopus plugins by combining daylight and energy values in algorithm-based optimization methods. With the available data, he determined that the daylight performance improved by about 40% and reduced energy consumption by about 28% among the data he obtained as a result of the study, and he revealed a method. In this context, this research has been examined in order to contribute to the article in terms of connecting the building orientation to parametric data.

Limitations and Assumption in the Case Study

This study proposes a decision support model to provide optimum orientation by evaluating the wind and vista components together for the new construction to

[13]Varoğlu, S. E. Sıcak iklim bölgelerindeki binaların optimum yönlenme ve optimum gölgelemesi için bir yöntem. (A method for optimum orientation and optimum shading of buildings in hot climate regions.) Yakın Doğu Üniversitesi, Fen Bilimleri Enstitüsü, Mimarlık Anabilim Dalı, Doctoral dissertation, 2017

[14]Topçu, C. Toplu konut planlamasında ekolojik yaklaşım önerileri Kiptaş Kayabaşı Toplu Konut Örneği. (Ecological approach suggestions in mass housing planning Kiptaş Kayabaşı Mass Housing Example.) T.C. İstanbul Aydın Üniversitesi, Lisansüstü Eğitim Enstitüsü, Mimarlık Anabilim Dalı, Mimarlık Programı, Master's Thesis, 2020.

[15]Turan, S. E. Kanal İstanbul mücavirinin mühendislik jeomorfolojisi. (Engineering geomorphology of Canal Istanbul adjacent.) İstanbul: Marmara Üniversitesi, Sosyal Bilimler Enstitüsü, Coğrafya Anabilimdalı, Master's Thesis, 2019

[16]Aksin, F. N. Yapı kabuklarının günışığı ve enerji bağlamında eniyilenmesinde parametrik modelleme ve evrimsel algoritma kullanımı. (Use of parametric modeling and evolutionary algorithms in optimizing building envelopes in terms of daylight and energy.) Ankara: Gazi Üniversitesi, fen bilimleri enstitüsü, mimarlık ana bilim dalı, Master's Thesis, 2019.

be formed within the Canal Istanbul impact area. It is known that the existing construction in the region will change after the canal is built and new structures will be built as a result of urban planning. Within the scope of this study, the canal project was investigated with an objective approach, and the climatic data of the region were revealed according to the information obtained from various sources. Using these data, a model was created to support the designer in the optimal orientation of the buildings to be built in the region in the context of vista and climatic conditions.

Using these data, a model was created to support the designer in guiding the new buildings to be built in the region. By determining the "predominant wind direction" and "optimal building direction" of the region, the canal vista factor was focused on for the orientation of the structures to be built on the canal route. In order to reveal the architectural structure, a building model was placed on the zoning plan announced by the state by parameterizing the number of floors, floor height and window width. The model is positioned in two directions according to the "closest" to the canal vista and the "last point" where the view can be seen, and the alternative orientations determined between these two directions are analyzed to measure how far the structure moves from the north and prevailing wind directions and how close it approaches the optimum direction. An "optimization experiment" was conducted to help determine the most ideal orientation over all the data obtained, and a "direction scoring" was tried to be revealed over the alternatives. In addition, only the natural air conditioning parameter is considered without using mechanical heating and cooling systems in the model.

Since the elevation of the region is 65 m on average and there is no significant elevation difference, the topographic slope of the region was ignored and not included in the calculations. Since a new landscape axis will be formed after the construction of the canal in the area, the orientation of the structures is limited to the view of the canal. Since the authorities in the region planned the construction to be horizontal architecture, the buildings in the model were considered as low-rise. It is known that the distance between the buildings is important, but due to the sparse construction strategy in the settlement close to the canal, a settlement pattern was not created and the analysis was evaluated on a single model. In the study, the effect of alternative building forms on the result was not taken into account. The focus is on optimum orientation of first-degree volumes, where the most time is spent.

Characteristic Investigation of the Canal Istanbul Project Area

In many countries in the world, artificial waterways that shorten the routes have been created in order to ease the sea transportation and to enable the ships to reach the desired point in a shorter time. The canals have been effective in changing the texture of the cities, as well as easing trade and transportation. Functionality is at the forefront as other canals such as Suez, Panama, Corinth, and Kiel were built to shorten the route. They have developed with industrial

construction rather than housing projects.[17] In the canal area planned to be built in Istanbul, it is stated as a project where a new construction process will be started and at the same time the largest smart city in the world will be established.[18]

Although the idea of creating an alternative waterway to the Bosphorus has been considered for many years, it has been announced that it is planned to be built in 2011. While the project, which will divide the European side into two, is being implemented, the foundation of the Sazlidere Bridge was laid in 2021 and the works were started in this way, before the canal excavation works started.[19]

Figure 1. *The Planned Route of Canal*[20]

In the EIA Report, 5 different alternative routes determined for the project were compared with each other in terms of economic, ecological and technical aspects. It was decided that the route starting from the isthmus separating the Marmara Sea from Kucukcekmece Lake, continuing along the Sazlidere Dam Basin, and then passing the Sazlibosna Village, reaching the east of Dursunkoy and passing the Baklali Village, reaching the Black Sea in the east of Terkos Lake. Canal; It is planned to have a length of 45 km, a floor width of 275 m and a canal depth of 20.75 m. On the route of the project as seen in Figure 1; It is stated that it

[17]WWF. "Ya Kanal Ya İstanbul" Kanal İstanbul Projesinin Ekolojik, Sosyal ve Ekonomik Değerlendirmesi. ("Either Canal or Istanbul" Ecological, Social and Economic Evaluation of Canal Istanbul Project.) İstanbul, 2015

[18]T.C. Çevre ve Şehircilik Bakanlığı. Bakan Kurum: "Kanal İstanbul Bir Devlet ve Millet Projesidir". (Minister Institution: "Canal Istanbul is a State and Nation Project".) Ekim 22, 2021. tarihinde csb.gov.tr, 2021. https://csb.gov.tr/bakan-kurum-kanal-istanbul-bir-devlet-ve-millet-projesidir-bakanlik-faaliyetleri-30900adresinden alındı

[19]DW. Kanal İstanbul'un ilk köprüsünün temel atma töreni yapıldı. (The groundbreaking ceremony of the first bridge of Canal Istanbul was held.) Ağustos 20, 2021 tarihinde www.dw.com: https://www.dw. com/tr/kanal-istanbulun-ilk-k%C3%B6pr%C3%BCs%C3%BCn%C3%BCn-temel-atma-t%C3%B6 reni-yap%C4%B1ld%C4%B1/a-58056499 adresinden alındı

[20]González, R. P. (2021, Nisan 29). Erdogan's "crazy" canal rejected by Turkish banks. Atalayar: https:// atalayar.com/en/content/erdogans-crazy-canal-rejected-turkish-banks adresinden alındı

will pass through the districts of Avcilar, Kucukcekmece, Basaksehir and Arnavutkoy.[21]

Murat Kurum, Minister of Environment and Urbanization of Turkey, said, "The project will be based on horizontal architecture, and healthy and safe living spaces will be planned at the human scale, protecting the ancient values, while at the same time eliminating the risk of disasters."[22]

The project area has been divided into 7 stages in order to plan the construction and landscaping, and the 3 stages of the area covering Basaksehir and Arnavutkoy districts have been approved as of 2021. It is stated that 52% of the total area in these stages is reserved for green areas, roads and social facilities. It has been announced that a ground floor and a maximum of 4 floors will be built for the housing projects to be built on the basis of horizontal architecture, and a total of 4 and 5 floors, including the ground floor, for the structures to be built in the social reinforcement areas, and high-rise buildings will not be allowed.[23] There is currently no focused landscape component in the region. It is thought that the landscape will be a water element in the orientation of the structures that are within sight of the canal.

The Catalca region, which has an undulating topography with an average elevation of 65 meters, shows similarity in the study area of the climate since there is no significant difference in elevation and aspect. It is stated that the temperature and precipitation values are average due to the fact that the region is surrounded by seas.[24]

Figure 2. *Main Climate Types of Turkey*

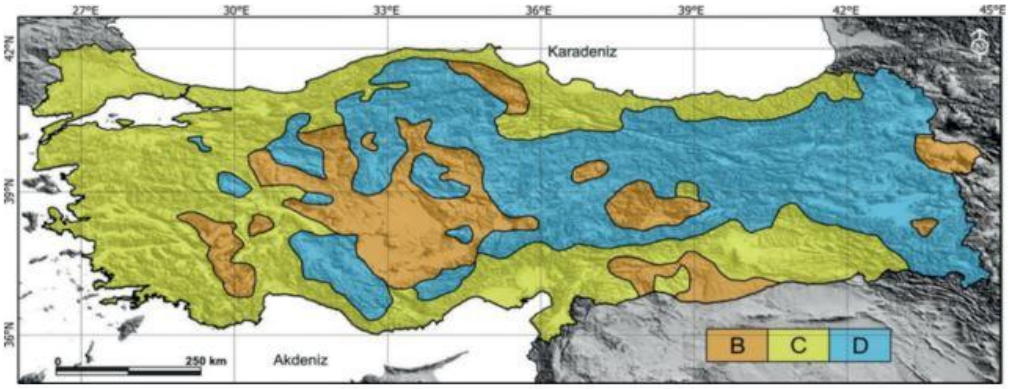

[21]Çınar Mühendislik Müşavirlik A.Ş. Kanal İstanbul projesi, çevresel etki değerlendirmesi raporu. (Canal Istanbul project, environmental impact assessment report.) Ankara: T.C. Ulaştırma ve Altyapı Bakanlığı, Altyapı Yatırımları Genel Müdürlüğü, 2019.

[22]Gündoğmuş, Y. N. (2018, Kasım 21). Ocak 3, 2021 tarihinde aa.com.tr: https://www.aa.com.tr/tr/turkiye/cevre-ve-sehircilik-bakani-kurum-kanal-istanbul-projesinde-yatay-mimari-esas-alinacak/1317357 adresinden alındı.

[23]T.C. Çevre ve Şehircilik Bakanlığı. (2020, Ocak 15). Akıllı Şehir Uygulamalarında İlk Örnek Kanal İstanbul Olacak. (Canal Istanbul will be the first example in Smart City Applications.) Ocak 2, 2021 tarihinde Türkiye Cumhuriyeti Çevre ve Şehircilik Bakanlığı: https://csb.gov.tr/akilli-sehir-uygulama larinda-ilk-ornek-kanal-istanbul-olacak-bakanlik-faaliyetleri-29695 adresinden alındı.

[24]Turan, S. E. Kanal İstanbul mücavirinin mühendislik jeomorfolojisi. (Engineering geomorphology of Canal Istanbul adjacent.) İstanbul: Marmara Üniversitesi, Sosyal Bilimler Enstitüsü, Coğrafya Anabilimdalı, Master's Thesis, 2019

Since Istanbul is surrounded by sea on three sides, it has natural ventilation corridors, and also has advantageous climatic features with its forested areas and different elevations. The Bosphorus also has an important effect on the formation of the natural air corridor.[25] Although it is stated in the literature that the prevailing climate in Istanbul is temperate-humid climate[26], as seen in figure 2, it is located in the temperate climate zone according to Koppen.[27] It is also stated in the literature that it has a transitional climate showing the effects of the Black Sea and the Mediterranean. In addition, it is observed that the winds coming from the north are the most effective.[28]

16-way wind data were obtained from Catalca Radar, Ataturk Airport, Istanbul Region and Kartal Meteorology stations. (Figure 2) As a result of this, first order prevailing wind directions; Catalca Meteorology Station has been determined as N (north) according to the blow numbers, Catalca Radar Meteorology Station has been determined as NE (northeast) according to the blow numbers, Ataturk Airport Meteorology Station has been determined as N (north) according to the blow numbers, and Istanbul Regional Meteorology Station has been determined as NE (northeast) according to the blow numbers.

Figure 3. *Wind Diagram According to Blow Numbers*

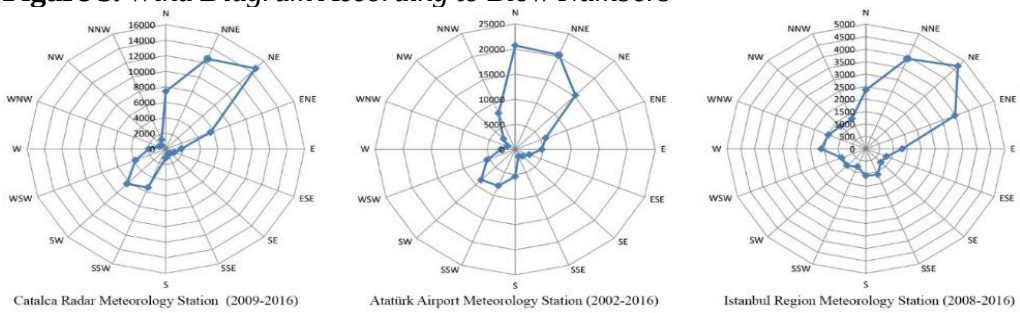

In the EIA Report (2019), a model study was conducted using 2014 data to determine the climatic characteristics of the project route (Figure 3). In this study, the wind blow numbers and speeds in the long-term bulletin obtained from Catalca Radar Station numbered 17047 in the northern part of the project and Florya Station numbered 17636 in the south of the project were compared with the monthly wind blowing numbers of the last 10 years. The first order prevailing wind direction of Catalca Radar Station was calculated as NE (northeast) with a

[25]Şimşek, Ç. K. "İstanbul'un mezo ve mikro iklimsel değişiminin kuzey ormanları ve kent içi yeşil alanlar ile ilişkisi." (The relationship of Istanbul's meso- and microclimatic change with northern forests and urban green areas.) In Ekosistem, İklim ve Kentsel Büyüme Perspektifinden İstanbul ve Kuzey Ormanları (s. 96-109). Türkiye Ormancılar Derneği, 2020.

[26]Ovalı, P. K. Biyoklimatik tasarım matrisi (Türkiye). (Bioclimatic design matrix (Türkiye).) Trakya Üniversitesi Mühendislik Bilimleri Dergisi 20, no. 2 (2019): 51-66.

[27]Özmen, E., and Ş. Beşiroğlu. "Aynı iklim sınıfında farklı iki ülkenin enerji etkin bina kavramı bağlamında ele alınması: İspanya ve Türkiye." (Considering two different countries in the same climate class in the context of the energy efficient building concept: Spain and Türkiye.) XIV. Mimarlıkta Sayısal Tasarım Ulusal Sempozyumu (2020): 129-140.

[28]Gürel, A., and A. E. Gündüz. İstanbul'un ekolojik yapısı üzerine bir araştırma. (A research on the ecological structure of Istanbul.) Marmara Sosyal Araştırmalar Dergisi 1 (2011)

blow number of 1531, NNE (north-northeast) with a second order blow number of 1513, and N (north) with a third-degree blow number of 1252. The same results were found for Florya Station.[29]

Turan (2019) determined the prevailing wind direction in the north of the canal as NNE (north-northeast) according to the data obtained from Kumkoy Station in the north and Florya Station in the south. In addition, he determined that the weather corridor is between NNE-SSW (north-northeast-south-southwest), although there are strong winds in the NNW (north-northwest) direction. He also stated that the dominant wind direction in the south of the canal is NNE (north-northeast).[30]

Although there are studies in the field of law about the project in the literature, studies in the field of "architecture" are almost non-existent. Within the scope of the article, researches on the ecology and physiology of the region were made and various data that could be input to architectural design were obtained. Based on these data, parametric and numerical design principles and methods were used in order to suggest the optimum building orientation in the structuring of the region. With these techniques, a "model" has been developed, taking into account the existing zoning plans of the region where there is no construction yet.

Model Recommendation

The Canal, which is planned to be positioned as an artificial waterway project in the direction of the north-south axis of the European side of Istanbul, has brought architectural activities to the agenda. In this project, which is in every architectural or urban planning organization, some planning for design and operation is required. In addition to the EIA report of the region, the zoning plans of 1000 and 5000 for the three regions were prepared and approved. The zoning plans developed with the focus of the canal route include areas of activity such as housing, trade and social centers.

As it is known, it is a very general design principle to determine various criteria for the settlement of architectural structures in parcels and to maintain optimum viewing directions according to these criteria.[31] In this study, "a model" has been experienced to provide optimum building orientation according to the above principles for the zones to be opened for construction in the canal region.

The stream formed in the region with the construction of the canal has been evaluated as the determining criterion in the orientation of the building, as it will

[29]Çınar Mühendislik Müşavirlik A.Ş. Kanal İstanbul projesi, çevresel etki değerlendirmesi raporu. (Canal Istanbul project, environmental impact assessment report.) Ankara: T.C. Ulaştırma ve Altyapı Bakanlığı, Altyapı Yatırımları Genel Müdürlüğü, 2019.

[30]Turan, S. E. Kanal İstanbul mücavirinin mühendislik jeomorfolojisi. (Engineering geomorphology of Canal Istanbul adjacent.) İstanbul: Marmara Üniversitesi, Sosyal Bilimler Enstitüsü, Coğrafya Anabilimdalı, Master's Thesis, 2019

[31]Baydoğan, M. Ç. Tip imar yönetmeliğine uygun vaziyet planı üreten bir yapay zeka destek sistemi. (An artificial intelligence support system that produces site plans in accordance with typical zoning regulations.) İstanbul: İstanbul Teknik Üniversitesi, Fen Bilimleri Enstitüsü, Mimarlık Anabilim Dalı, Mimari Tasarım Programı, Doctoral dissertation, 2013

present a new "strait" appearance. In addition to this parameter, which is called "landscape direction" in the architectural literature, the "energy performance" of the buildings is also taken into consideration as a control parameter in the secondary plan. It is aimed to provide optimization in building orientation by establishing mathematical relations between "optimum direction", "prevailing wind direction" and "north direction". In this respect, the model provides an opportunity for the designer to evaluate alternatives in deciding the building orientation by producing correlations between design and ecological approaches.

Determining Input Data for the Model

The data needed to find the optimum building direction in the ecological context of the buildings planned to be built in the Canal Istanbul project area were determined. Alternative "output data" is produced by using design and ecological "input data" for the model to operate. In this sense, it is important to determine and reveal the input data. Input data can be listed as building floors, prevailing wind direction, optimum direction, plan of the building, coordinate of the building, axis of the canal, viewing angle and spline lengths of the vista. The detection stages of each input data are as follows:

Building Floors

The construction in the region -as mentioned above- has been described as "horizontal architecture" by the authorized institutions. In this respect, it has been evaluated that the construction will be in the form of maximum 5-storey buildings. According to these data, the buildings to be used in the model are limited to 2-5 floors.

Prevailing Wind Direction

In the second part of the research, the physical and ecological characteristics of the region were revealed. According to these data, the prevailing wind direction in the Northern parts of the region was accepted as NE (Northeast) and the prevailing wind direction in the South coasts was NNE (North-Northeast).

Table 1. *Prevailing Wind Directions of the Region According to the EIA Report*[32]

Section	Prevailing wind direction	Angle with north
Northern section	NE (Northeast)	202.5^0
South section	NNE (Northnortheast)	225^0

In this case, the prevailing angle of incidence of the wind in the northern parts of the region with respect to the North is 202.50, and in the southern parts, the prevailing angle of incidence relative to the North is added to the calculations as 2250 (Table 1).

[32]Çınar Mühendislik Müşavirlik A.Ş. Kanal İstanbul projesi, çevresel etki değerlendirmesi raporu. (Canal Istanbul project, environmental impact assessment report.) Ankara: T.C. Ulaştırma ve Altyapı Bakanlığı, Altyapı Yatırımları Genel Müdürlüğü, 2019

Optimum Direction

The region is located in the "Temperate-Humid Climate" zone. Optimum building direction ranges of the temperate-humid climate zone are shown in Table 2.

Table 2. *The Optimum Building Orientation Diagram for the Temperate-Humid Climate Zone*[33]

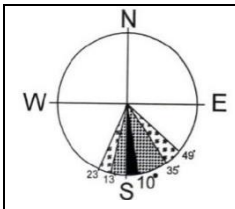	1. Angle range	2. Angle range	3. Angle range
	Between 0^0-10^0	Between 13^0-35^0	Between 23^0-49^0

According to the research, between 00-100 is accepted as the optimum direction range. Between 130-350 is considered as the "secondary" and between 230-490 as the "tertiary" optimum direction range. This diagram, which Ovali brought to the literature as a result of their research, was accepted as a reference for the "optimal direction" in the study and the angular values on it were added to the calculations as input parameters (Table 2).

Figure 4. *Canal Axis (a), Building Coordinate (b) and Building Plan (c)*

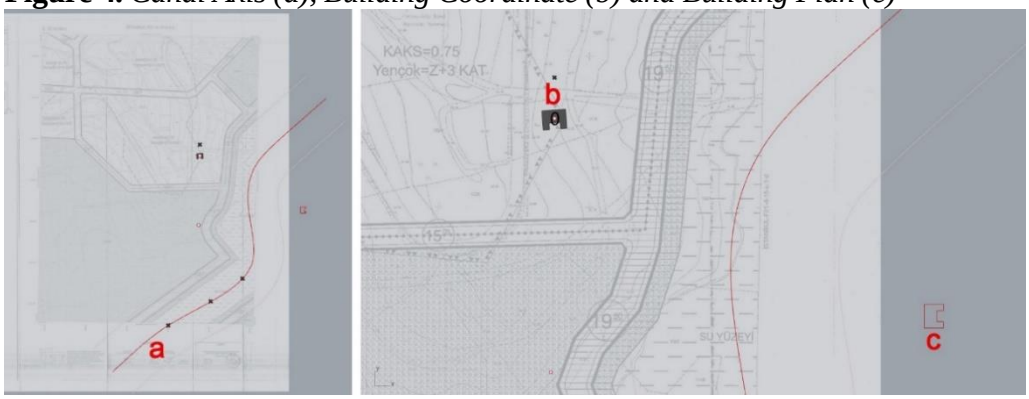

Plan, Coordinate of the Building and Axis of the Canal

The developed model is designed with the ability to measure for the structure to be applied to any point of the study area. For this, first of all, the zoning plan of the region is visually transferred to Rhinoceros3D software. Then the water axis of the canal is drawn with a "spline" object. Afterwards, the plan projection of the building to be applied is determined by a "polyline" object and its coordinates by a "point" object. With these inputs, it is possible to work on real data (Figure 4).

[33]Ovalı, P. K. *Türkiye iklim bölgeleri bağlamında ekolojik tasarım ölçütleri sistematiğinin oluşturulması "Kayaköy yerleşmesinde örneklenmesi".* (Establishing a systematic of ecological design criteria in the context of Turkey's climate zones "Exampling in Kayaköy settlement".) Edirne: T.C. Trakya Üniversitesi, Fen Bilimleri Enstitüsü, Mimarlık Anabilim Dalı, Doctoral dissertation, 2009

Figure 5. *The Seen Vista Spline (a) and the Perpendicular Length to the Vista (b)*

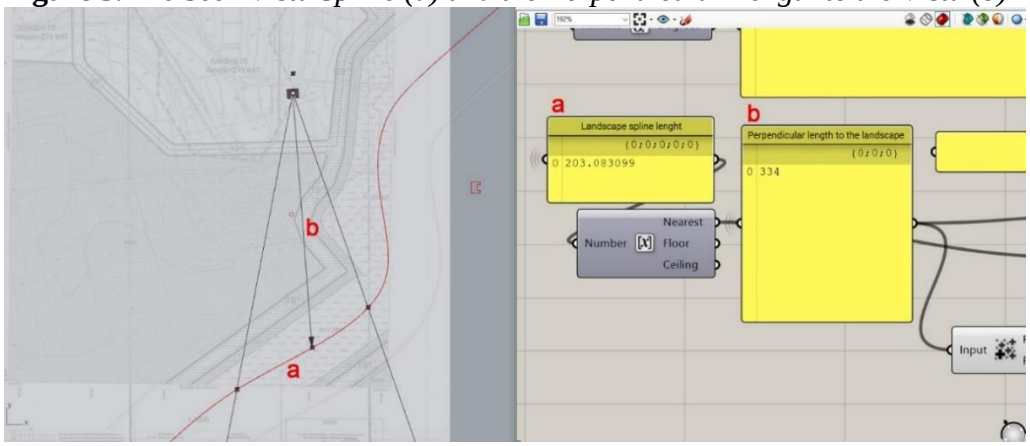

Angle of View and View Spline Lengths

The determined data is transferred to Grasshopper3D, a Rhinoceros3D plugin. Using these data, it calculates the spline length it sees according to the coordinate and orientation of the structure. In the calculation, the "view angle" is parameterized to determine the building's point of view. In this way, the potential differences that the viewing angle, which changes according to different window widths, will create in the seen vista spline, is also taken under control. In addition to this spline length, the "vertical view distance to the vista" of the building is also calculated as an input data (Figure 5).

Figure 6. *Grasshopper3D Screen where the Model is Developed*

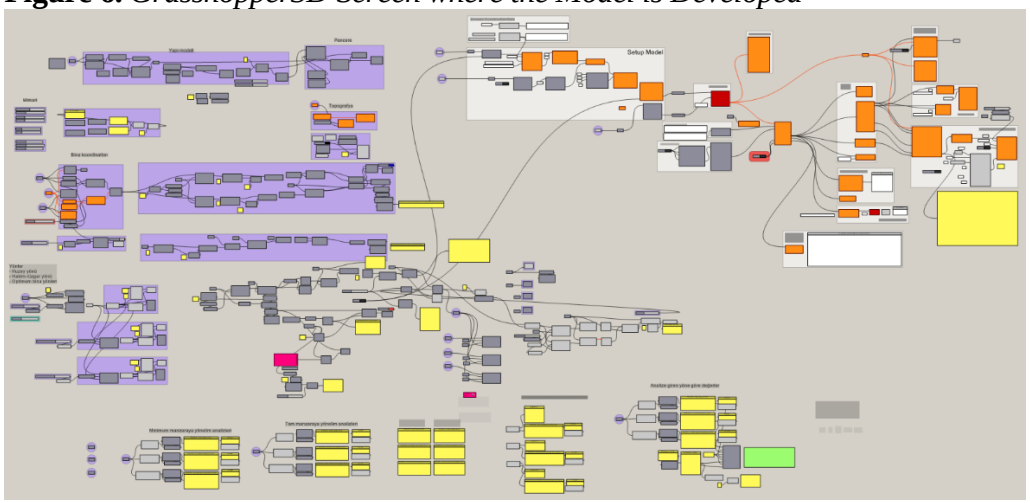

Development of the Model

With its parametric structure, Grasshopper3D has been evaluated as an ideal data processing platform in this research, as in many similar studies. In this context, a script was developed as a model to process the input data in the Grasshopper3D medium (Figure 6).

Figure 7. *Overlaying the Plan Contour on the Zoning Plan and Parameterizing the Architectural Components*

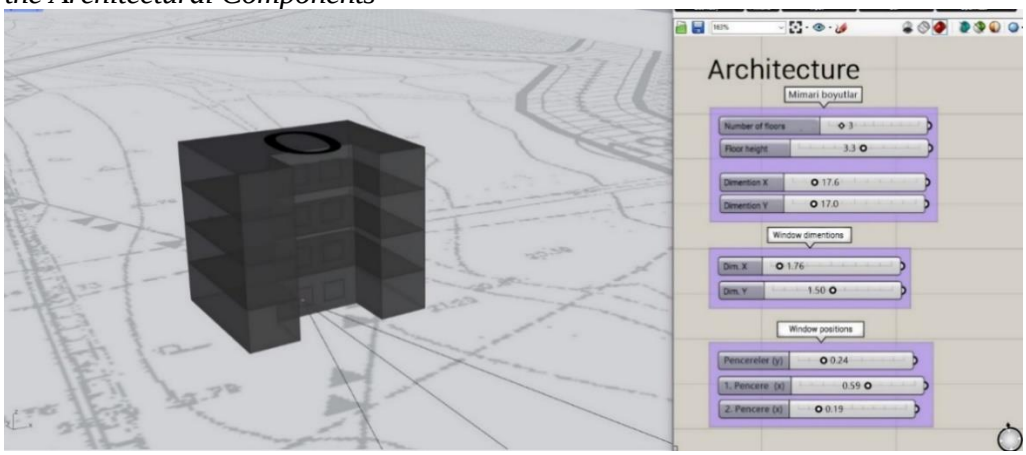

First of all, the plan contour is superimposed on its point position on the zoning plan and the building model is produced. At this stage, the number of floors, floor height and window width of the building are parameterized. The aim here is to enable the model to calculate buildings in each plan type according to their different characteristics (Figure 7).

Table 3. *Layering of the structural components used in the model*

Parameter Name	**Description**	**Value**
U Exterior Wall	Conductivity of the walls	0,599 W/m^{2}K
U_Window	Conductivity of the windows	1,687 W/m^{2}K
U Roof	Conductivity of the roof(top)	0,208 W/m^{2}K
U Interior Floor	Conductivity of the interior slabs	2,014 W/m^{2}K
U Ground Floor	Conductivity of the ground slab	0,394 W/m^{2}K
Activity	Activity Conditions of Building	Midrise Apartment Occupancy: 0,04 p/m^2 Clo: 1,0 Met: 0,90 met
HVAC Settings	Building HVAC Conditions	(Variable air Volume) chiller gas boiler reheat

The intended structural characteristics for the building models used in the analysis are provided in Table 3. For the model, the total thermal transmittance (U-value) of the external wall layer was taken as 0.599 W/m2- K, the internal floor as 2.014 W/m2-K, the roof as 0.208 W/m2-K, and the windows as 1.687 W/m2-K. Additionally, it was assumed that each analyzed building had mechanical HVAC systems using “VAV (Variable air Volume) chiller gas boiler reheat”.

Figure 8. *Establishing the Correlation between North Direction (A), Prevailing Wind Direction (B) and Optimum Building Directions (C)*

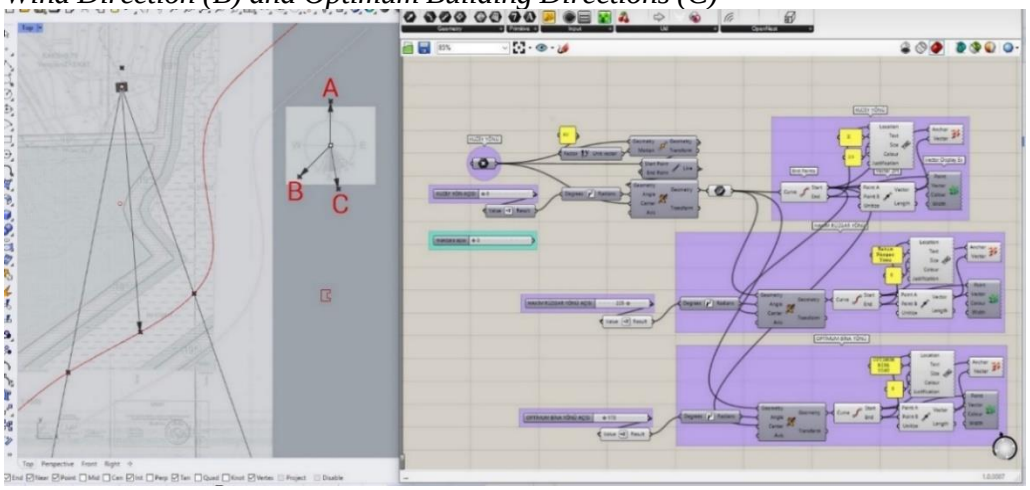

Afterwards, a mathematical relation was established between "North direction", "prevailing wind direction" and "optimal building directions" considering the input data determined above. By parameterizing this relation, it is possible to process data that varies according to any region of the canal area. For example, while the wind direction is NE in the northern parts of the canal axis, it is NNE in the southern parts. This difference in between can be processed into the system via Grasshopper3D over the angle of the wind with the north (Figure 8).

Figure 9. *The Section Developed with the LadyBug Plugin*

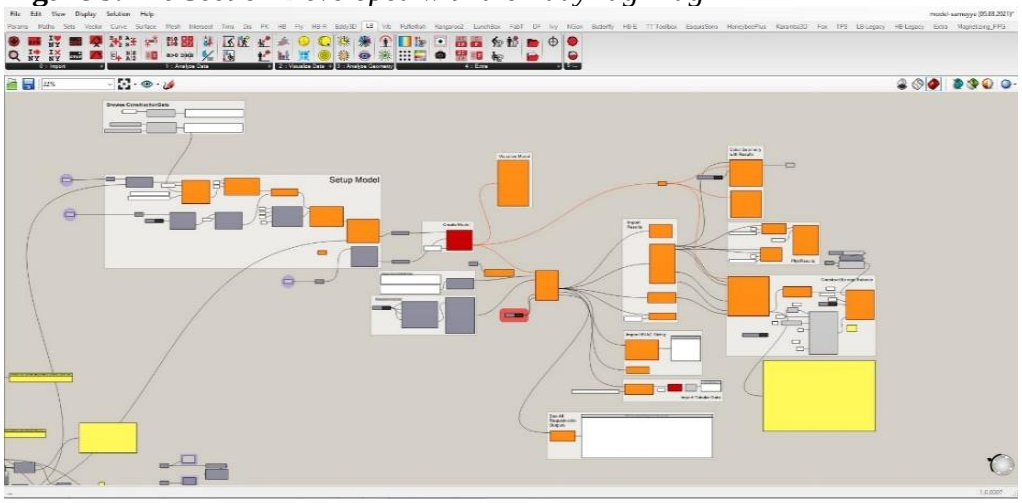

In addition, another section has been considered in Grasshopper3D by using the LadyBug plugin in order to compare the amount of energy consumption according to alternative building orientations. This section was developed based on the residential/ apartment type building with a wall thickness of 25 cm and the Istanbul, Yeşilköy EPW file obtained from Energyplus. Alternative plan types, window sizes and floor elevations are other input parameters used in this section (Figure 9).

Operation of the Model

The model first reveals the building form according to the number of floors and window sizes over the determined plan contour and location. It then makes the user select the "canal axis". It expects the region (North or South) to be preferred in order to calculate the prevailing wind direction from behind. After these initial inputs are completed, the system determines "two directions" by positioning the building according to the "closest" point to the vista and the "furthest" point, which is the last distance from which the vista can be seen. Then, it determines intervals according to the number of analyzes from the area between these two directions and extracts alternative orientations. Each orientation intersects with a slice of the vista spline according to the conical point of view. The system makes calculations on both these intersecting curves and the viewing distances to the vista, and translates how much each orientation benefits from the vista into mathematical data.

According to the vista factor, these alternative orientations of the building are transferred to another analysis to be compared on the "prevailing wind direction", "north direction" and "optimal directions". At this stage, it is measured how far the building moves from the north and prevailing wind directions and how close it is to the optimum direction. Then, in the section added to the system with the "LadyBug" plugin, energy consumption calculations are made for each alternative orientation. The data obtained after all these calculations are presented to the user in the form of a table in order to be able to choose among alternative orientations.

Calculation Examples

Figure 10. *Determination of Nearest (a), Farthest (b) and Intermediate Directions (c) for A and B Position*

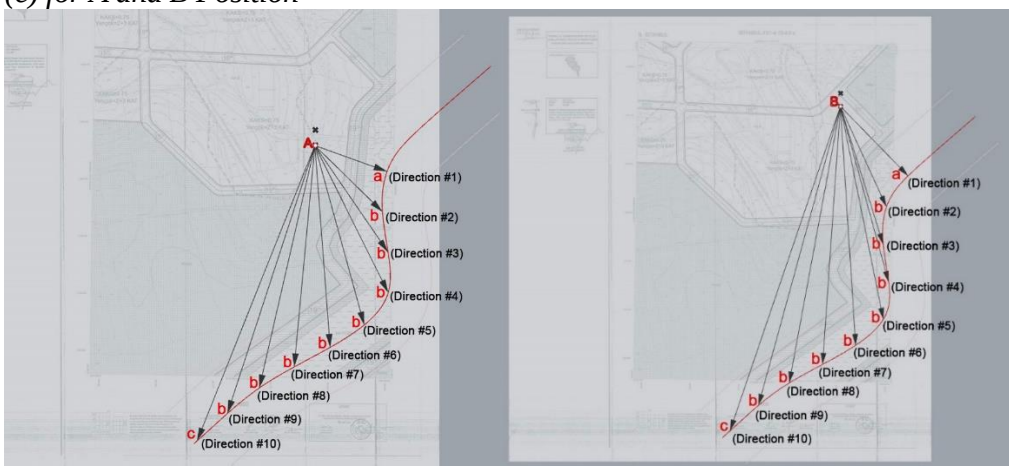

Table 4. *Data Obtained from the Orientation of the Structure According to 10 Different Angles and Two Different Locations*

Directions (Position A)	With the North direction (Degrees)	Deviation from the optimum direction (Degrees)	With the prevailing wind direction (Degrees)	Distance perpendicular to the vista (Meters)	The seen vista spline (Meters)	District Cooling (kWh)	District Heating (kWh)	Energy Per Conditioned Building Area (kWh/m^2)
Dir. #1	110^0	60^0	93^0	127	71	4677.08	6875.79	76.62
Dir. #2	134^0	36^0	68^0	156	148	4333.27	6291.44	70.46
Dir. #3	146^0	24^0	57^0	214	193	3975.75	6002.61	66.18
Dir. #4	154^0	16^0	49^0	272	206	3712.10	5829.64	63.28
Dir. #5	165^0	5^0	38^0	307	192	3402.23	5659.16	60.09
Dir. #6	176^0	6^0	27^0	334	203	3224.11	5588.13	58.44
Dir. #7	185^0	15^0	17^0	367	275	3098.95	6162.43	56.50
Dir. #8	193^0	23^0	10^0	411	262	3150.17	6210.45	57.10
Dir. #9	198^0	28^0	4^0	466	227	3213.22	6262.11	57.80
Dir. #10	202^0	32^0	1^0	525	199	3277.02	6315.61	58.52
Directions (Position B)	With the North direction (Degrees)	Deviation from the optimum direction (Degrees)	With the prevailing wind direction (Degrees)	Distance perpendicular to the vista (Meters)	The seen vista spline (Meters)	District Cooling (kWh)	District Heating (kWh)	Energy Per Conditioned Building Area (kWh/m^2)
Dir. #1	136^0	34^0	67^0	188	104	4171.04	6794.52	66.90
Dir. #2	155^0	15^0	47^0	215	299	3571.93	6381.59	60.72
Dir. #3	163^0	7^0	40^0	281	343	3344.57	6259.08	58.59
Dir. #4	165^0	5^0	38^0	354	354	3298.52	6235.83	58.16
Dir. #5	169^0	1^0	34^0	422	376	3219.42	6198.48	57.45
Dir. #6	176^0	6^0	26^0	465	408	3127.80	6161.02	56.67
Dir. #7	184^0	14^0	19^0	502	371	3097.52	6159.57	56.47
Dir. #8	190^0	20^0	12^0	546	325	3123.41	6187.37	56.80
Dir. #9	195^0	25^0	7^0	602	279	3172.77	6228.96	57.36
Dir. #10	199^0	29^0	4^0	666	244	3228.16	6274.50	57.97

Two example calculations are presented in Table 4. For these examples, a point close to the Southern parts of the canal was chosen as the location of the structures. As can be seen in Figure 10, a total of 10 alternative directions were determined, with the closest and farthest perpendicular points to the vista axis. The resulting values from each orientation are shown in the table. According to the data, for example, orientation number 6 at position A is the most concealed orientation from the North direction compared to the others, and it is one of the orientations closest to the "optimal direction".

In this orientation, there is a 27 degree angle difference between the structure and the prevailing wind direction of the region. Assuming that zero (0) degree is the most sheltered orientation from the prevailing wind, it is thought that the value obtained can give an idea about the success of the orientation. In this 6 orientation, the building has a vertical vista distance of 334 m and the spline it sweeps as a vista is 203 m. As another example, it can be said that orientation number 5 in position B has the least amount of deviation from the optimum direction compared to the others. However, this direction is far behind in terms of vertical distance orientation to the vista.

It is thought that similar evaluations made on these data can give the user an idea for an ideal orientation. However, it is predicted that connecting these data to a certain set of mathematical rules and thus directing a quantitative evaluation will

be a more accurate and scientific trend in the decision-making process. In this context, an "optimization experiment" was conducted to help determine the optimum orientation over all the data obtained, and a "direction scoring" was tried to be put forward through the alternatives.

Optimization Experiment

Figure 11. *Conversion of All Values to Percentages on Grasshopper3D*

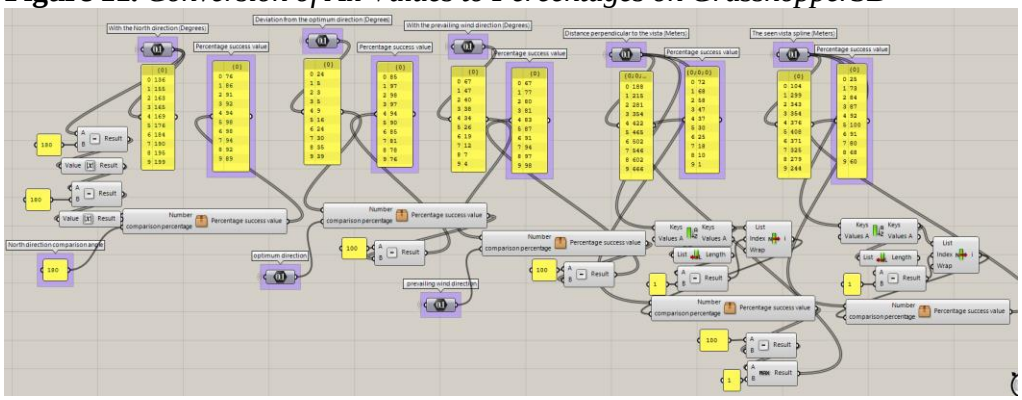

First of all, this issue was approached as a multivariate function. A value calculation over 100 points was made for all the data obtained. According to this calculation, the orientation with the most hidden front from the North direction approached 100 points more. Likewise, the orientation closest to the optimum direction and the orientation most hidden from the prevailing wind direction also approached 100 points in their own field. In addition, the direction with the closest vertical orientation to the vista and the orientation with the most vista spline were also rated within themselves and approached 100 points (Figure 11).

Table 5. *Percentage Success Values of the Obtained Data*

Directions (Position A)	Hiding from the north (Degrees)	Deviation from the optimum direction (Degrees)	With the prevailing wind direction (Degrees)	Distance perpendicular to the vista (Meters)	The seen vista spline (%)
Direction #1	61	69	54	76	26
Direction #2	74	84	66	70	54
Direction #3	81	91	72	59	70
Direction #4	86	96	76	48	75
Direction #5	92	97	81	42	70
Direction #6	98	90	87	36	74
Direction #7	97	84	92	30	100
Direction #8	93	79	95	22	95
Direction #9	90	76	98	11	83
Direction #10	88	74	100	1	72

Directions (Position B)	Hiding from the north (Degrees)	Deviation from the optimum direction (Degrees)	With the prevailing wind direction (Degrees)	Distance perpendicular to the vista (Meters)	The seen vista spline (%)
Direction #1	76	85	67	72	25
Direction #2	86	97	77	68	73
Direction #3	91	98	80	58	84
Direction #4	92	97	81	47	87
Direction #5	94	94	83	37	92
Direction #6	98	90	87	30	100
Direction #7	98	85	91	25	91
Direction #8	94	81	94	18	80
Direction #9	92	78	97	10	68
Direction #10	89	76	98	1	60

In Table 5, an example calculation is presented based on the data obtained from points A and B. In this calculation, in the comparison of "Hiding from the north" in the second column, it was examined how much the orientations reflect the 180-degree difference between them and the North direction. Likewise, in the comparison of "Deviation from the optimum direction" in the third column, the amount of directions approaching 160, which is the optimum direction degree of the Temperate- Humid Climate, was examined. In the fourth column, the question of how much the directions are hidden from the prevailing wind direction was converted into a score out of 100. In the fifth column, 1 point is given to the furthest point where the building placed on the point has a perpendicular view to vista, and other directions are scored according to this furthest direction. In the last column, each direction is scored by making a ratio according to the length of the spline that intersects the area scanned by the conical point of view. According to this approach, the success of the first orientation at point A with 110 degrees from the North direction is 61%. However, the success rate of orientation 6, whose angle with the North is 176 degrees on the same point, is 98%. According to this calculation, it can be said that orientation number 6 is 37% more successful than orientation number 1 in terms of "Hiding from the north".

In the next step, all percentages obtained are compared with each other in order to compare these new data and reach an average "success score" for each orientation. At this stage, it is left to the user to determine the percentage values to be used in comparison of all data (Figure 12). This is because the component that each user prioritizes is "subjective". For example, according to some users, being closer to the vista may be a priority and valuable because the spline distance of the vista is longer. Or, the optimum orientation may override the prevailing wind direction factor, according to some users.

Figure 12. *Obtaining the Average Success Score by Proportioning the Data with Each Other in Grasshopper 3D*

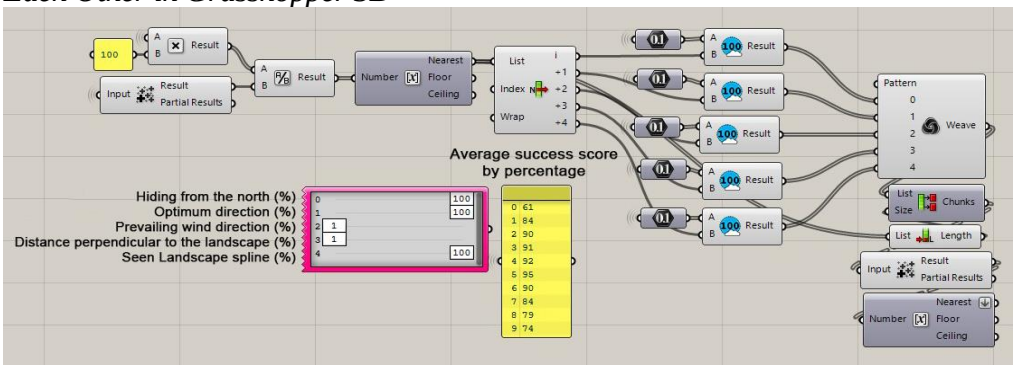

Table 6. *Success Scores Obtained as a Result of the Preferences of 4 Different Users*

Directions (Position A)	User #1's achievement score (%)	User #2's achievement score (%)	User #3's achievement score (%)	User #4's achievement score (%)
Values entered	%100-%100-%100-%100-%100	%100-%100-%1-%1-%100	%1-%100-%1-%100-%1	%8-%50-%10-%80-%50
Direction #1	57	51	71	60
Direction #2	70	70	75	70
Direction #3	75	80	74	72
Direction #4	76	85	71	71
Direction #5	76	85	68	67
Direction #6	77	86	62	65
Direction #7	81	93	56	68
Direction #8	77	88	49	62
Direction #9	72	82	43	53
Direction #10	67	77	37	46

Directions (Position B)	User #1's achievement score (%)	User #2's achievement score (%)	User #3's achievement score (%)	User #4's achievement score (%)
Values entered	%100-%100-%100-%100-%100	%100-%100-%1-%1-%100	%1-%100-%1-%100-%1	%8-%50-%10-%80-%50
Direction #1	65	61	77	64
Direction #2	80	84	81	79
Direction #3	82	90	76	78
Direction #4	81	91	71	74
Direction #5	80	92	64	71
Direction #6	81	95	59	69
Direction #7	78	90	54	64
Direction #8	73	84	49	57
Direction #9	69	79	43	50
Direction #10	65	74	38	43

In Table 6, the preference of sample percentage values belonging to four different users and the success scores for each orientation are given.

In the "Values entered" line in the table, respectively;

- Angle preference ratio with the north direction
- Angle preference ratio between optimum direction,
- Angle utilization ratio with the prevailing wind direction,
- Rate of use perpendicular to the vista,
- and the vista spline length utilization rate,

is shown as the preferred percentile.

Accordingly, it is seen that the first user at point A prefers each value equally. As a result of this preference, direction #7 is the most successful direction with 81%. It is observed that the second user wants to hide the building at the maximum level from the North side and bring it as close to the optimum direction as possible. In addition, it is understood that this user does not care about the prevailing wind direction and the proximity of the perpendicular view distance to the vista, but still wants to see the vista arc at the maximum level. As can be seen in the table, 93% success rate is again direction #7 responding to these preferences. The third user, on the other hand, does not seem to be interested in other values that want to aim as much as possible in the optimum direction and to have maximum vertical closeness to the vista. Again, as seen in the table, it is observed that Direction #2 meets these preferences with a success rate of 75%. It is seen that Direction #7 responds to the preferences of the fourth example user, followed in the table, with a success rate of 68%. In the columns below, the calculation of the same user values over the B point is shared. The results are as seen.

Figure 13. *Annual Heating-Cooling and annual energy data of Alternative Orientations in Position A*

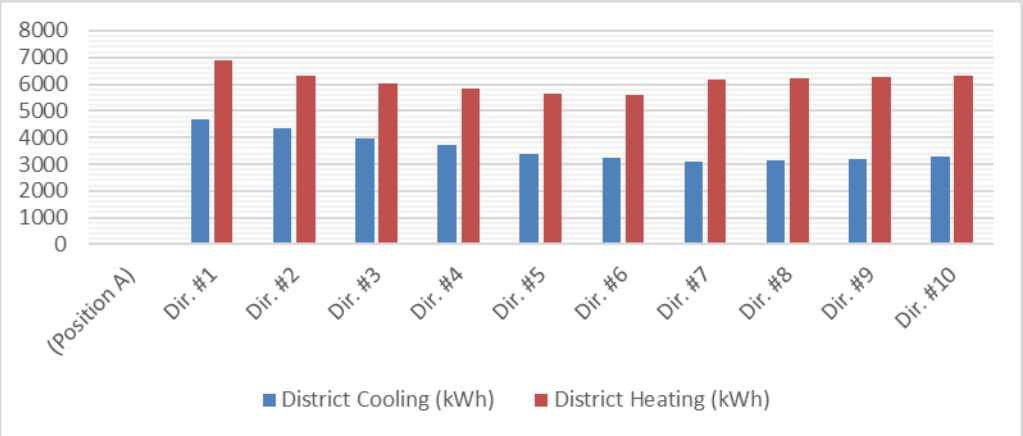

When the orientation states of which energy analysis is made in the case of Table 6 Position A are examined, the orientation situation that gives the best result in terms of cooling energy expenditure in summer energy efficiency is direction #7 with 3098.95 kWh. When the heating energy expenditure performances of the orientation alternatives are examined for the winter period, it is seen that the orientation alternative showing the lowest energy expenditure is direction #6 with 5588.13 kWh. Direction #6 is the orientation alternative that makes the closest

angle to the south direction with 176°. As the tendency towards the south in the winter period increases, the effect of solar radiation on the structure increases, thus creating a positive effect in terms of heating energy load. Direction #6 has a lower energy consumption in terms of heating energy load as it has a greater angular proximity to the south direction compared to other orientation alternatives (Figure 13).

Figure 14. *Annual Heating-Cooling and Annual Energy Data of Alternative Orientations in Position B*

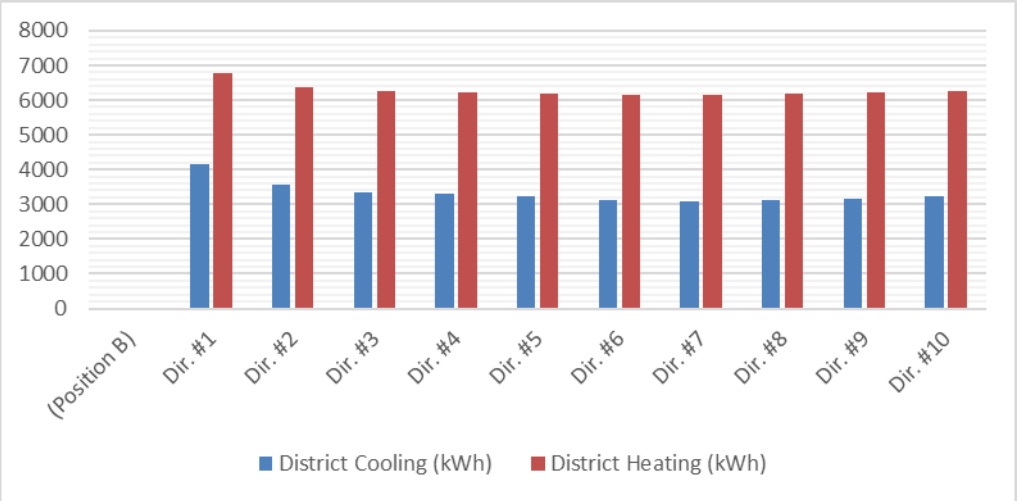

When the orientation states of which energy analysis was made in the case of Table 6 Position B are examined, the orientation situation that gives the best result in terms of cooling energy expenditure in summer energy efficiency is direction #7 with 3097.52 kWh. When the heating energy expenditure performances of the orientation alternatives are examined for the winter period, it is seen that the orientation alternative showing the lowest energy expenditure is direction #7 with 6159.57 kWh. Direction #8 is the orientation alternative that makes the closest angle to the south direction with 184°. As the tendency towards the south in the winter period increases, the effect of solar radiation on the structure increases, thus creating a positive effect in terms of heating energy load. Direction #6 has a lower energy consumption in terms of heating energy load since it has a greater angular proximity to the south direction compared to other orientation alternatives (Figure 14).

Conclusion

In recent years, environmentally sensitive building designs have been given more importance in the world than in the past, and various studies have been carried out in this field. Ways to get maximum efficiency with minimum damage from nature are being researched by designers with this sensitivity. With the increase in the human population, the change in the perception of comfort or the effect of industrialization, the amount of permeable surface is decreasing while the construction is increasing day by day. While the haphazard positioning of the

buildings causes more energy consumption and creates environmental pollution, it is possible to provide thermal comfort by directing the building according to the climatic conditions of the region. While the necessity of directing the building mass in the most appropriate way is obvious, the "vista" factor, which is an important user expectation, stands before us as another parameter that should be taken into account.

In this study, an "optimization model" has been developed by using parametric and numerical design principles in order to suggest the optimum orientation of the houses planned to be built within the project impact area according to their locations.

First of all, the current status of the project idea was investigated and the technical and ecological data of the project area were accessed. In these examinations made for the production of input parameters for the model developed within the scope of the study, "prevailing wind direction" and "optimal building direction" were determined by using the temperature and wind data of the region. Afterwards, the "vista" factor, which is an important component in the orientation of the buildings, was focused on and this factor was considered as a sub-context. As it is known, the vista has a complex structure with many parts and its valuation may vary from person to person. In this sense, it can be said that it is a very difficult component to determine based on quantitative data from a mathematical point of view. In the study, the vista was expressed with a "spline object" and was included in the model by being limited to two parameters: "closeness to the vista" and "spline of the seen vista".

A and B directions to give the user an ideal orientation idea; It has been analyzed with the data of hiding from the north, deviation from the optimum direction, the angle between the prevailing wind direction and the seen spline of the vista. Alternative directions are derived on the model, vista spline and analyzes are made for each direction in the ecological/climatic contexts mentioned above. Afterwards, it offers an approach in which user priorities are taken into account for the optimization of the data obtained as a result of the analysis.

In this study, the data obtained from the optimization were evaluated according to four different users and the success scores obtained as a result of the preferences were obtained. The most successful orientation according to users for location A; Direction #7 for the first user, direction #7 for the 2nd user, direction #2 for the 3rd user, and direction #5 for the user 4. For position B; Direction #3 for User 1, direction #6 for User 2, direction #2 for User 3, and direction #2 for User 4 was determined to be the most successful orientation. The study has been tested for alternative aspects and different users, and it has answered the expectation as a decision support model.

The project, which is thought to be a new construction area with the development of these and similar systems, is clear that ecologically efficient and environmentally sensitive structures or building orientations can be realized. It is thought that this study has a unique quality, especially in terms of intersecting this ecological sensitivity with the "vista" component. The study, which touches on a very wide research area, was kept within certain limits, as summarized above.

First of all, the "constraint" elements of the vista were ignored in the study. In

order to get more accurate results, the vista components should be reviewed and the mathematical differences that these components will make on the system should be investigated.

It is thought that large-scale land use projects will cause urban heat island. In this context, the possibility of possible heat islands that will occur on a large scale of construction should be evaluated and the model developed within the scope of the article should be reviewed in this respect and its algorithm should be re-established. It is thought that considering the building orientation in the area together with the energy efficient building understanding is important in terms of sustainability. It is predicted that the developed model will yield more accurate results by reinterpreting it according to this association.

Migration from rural areas to cities is expected to continue in the world. If the population is not 500,000 as planned after the project, the building decisions should be reviewed and it is recommended to reevaluate the parameter inputs of the model developed with the increase in the housing areas required for the population to reside in the future studies. Since it is planned to have a large population mobility in the region after the construction, it should be investigated whether it will affect the climatic characteristics. The developed model should be revised according to these studies and new input parameters should be constructed.

The model developed within the scope of the study takes into account the climatic data and interprets the ideal building orientation through these data. In this context, the model should be reinterpreted after the landscape project of the project area is clarified, taking into account the possible changes in the climate of the plant population added to the area. It is thought that the sea breezes will not be interrupted with the recreation areas to be created by the sea after the project, and it is stated by the ministry that the construction will be built on the basis of horizontal architecture. In this context, it is recommended to consider the shared literature in determining the input parameters for the number of floors to be used in the developed model.

Calculations in the developed model were made on the planar canal close settlements of the project area. The algorithm of the model should be re-established by adding topographic data. The model created is designed to measure every building form. Considering these definitions in the literature on the ideal building form, the effect of the building form to be used in the model on the results should also be investigated. The distance factor between buildings was not taken into account in this study. However, it is presented as information in terms of guiding future studies.

The model developed within the scope of the article can measure on every building form. However, in this study, analyzes were not made on alternative forms. Considering this and similar literature information shared, the model, climate zone-building form intersection should also be investigated.

Bibliography

Aksin FN (2019) *Yapı kabuklarının günışığı ve enerji bağlamında eniyilenmesinde parametrik modelleme ve evrimsel algoritma kullanımı.* (Use of parametric modeling and evolutionary algorithms in optimizing building envelopes in terms of daylight and

energy.) Ankara: Gazi Üniversitesi, fen bilimleri enstitüsü, mimarlık ana bilim dalı, Master's Thesis, 2019.

Balcıoğlu A (2019) *Geleneksel ve modern bağ evi örneklerinin soğutma enerjisi korunumunda etkili olan tasarım değişkenleri açısından değerlendirilmesi.* (Evaluation of traditional and modern vineyard house examples in terms of design variables effective in cooling energy conservation.) İstanbul: İstanbul Teknik Üniversitesi, Fen Bilimleri Enstitüsü, Mimarlık Anabilim Dalı, Çevre Kontrolü Ve Yapı Teknolojileri Programı, Master's Thesis, 2013.

Baydoğan MÇ (2013) *Tip imar yönetmeliğine uygun vaziyet planı üreten bir yapay zeka destek sistemi.* (An artificial intelligence support system that produces site plans in accordance with typical zoning regulations.) İstanbul: İstanbul Teknik Üniversitesi, Fen Bilimleri Enstitüsü, Mimarlık Anabilim Dalı, Mimari Tasarım Programı, Doctoral dissertation, 2013.

Çınar Mühendislik Müşavirlik AŞ (2019) *Kanal İstanbul projesi, çevresel etki değerlendirmesi raporu.* (Canal Istanbul project, environmental impact assessment report.) Ankara: T.C. Ulaştırma ve Altyapı Bakanlığı, Altyapı Yatırımları Genel Müdürlüğü, 2019.

Çobanyılmaz P, Yüksel ÜD (2013) "Kentlerin iklim değişikliğinden zarar görebilirliğinin belirlenmesi: Ankara örneği." (Determining the vulnerability of cities to climate change: Ankara example.) *Süleyman Demirel Üniversitesi Fen Bilimleri Enstitüsü Dergisi* 3, no. 17 (2013): 39-50.

DW (2021) *Kanal İstanbul'un ilk köprüsünün temel atma töreni yapıldı*. (The groundbreaking ceremony of the first bridge of Canal Istanbul was held.) Ağustos 20, 2021 tarihinde www.dw.com: https://www.dw.com/tr/kanal-istanbulun-ilk-k%C3%B6pr%C3%BCs%C3%BCn%C3%BCn-temel-atma-t%C3%B6reni-yap%C4%B1ld%C4%B1/a-58056499 adresinden alındı.

González RP (2021) *Erdogan's "crazy" canal rejected by Turkish banks*. Atalayar, 2021. https://atalayar.com/en/content/erdogans-crazy-canal-rejected-turkish-banksadresinde nalındı.

Gündoğmuş YN (2021) tarihinde aa.com.tr, 2018. https://www.aa.com.tr/tr/turkiye/cevre-ve-sehircilik-bakani-kurum-kanal-istanbul-projesinde-yatay-mimari-esas-alinacak/1317357 adresinden alındı.

Gürel A, Gündüz AE (2011) İstanbul'un ekolojik yapısı üzerine bir araştırma. (A research on the ecological structure of Istanbul.) *Marmara Sosyal Araştırmalar Dergisi* 1.

Kesici Ö (2019) "İstanbul Boğazı varken neden kanal istanbul?" (Why Canal Istanbul when there is the Bosphorus?) 4. In *Uluslararası Bilimsel Araştırmalar Kongresi* (s. 227-252). Ankara: Sosyal Bilimler, 2019.

Keskin K, Engin N (2019) "Toplu konutlardaki yerleşim kararlarının enerji etkin mimarlıktaki rolü." (The role of layout decisions in mass housing in energy efficient architecture.) *Mimarlık ve Yaşam Dergisi* 4, no. 1 (2019): 69-78.

Mangan SD (2006) *Akıllı binalarda alt sistem değerlendirmesi: İstanbul örneği.* (Subsystem evaluation in smart buildings: Istanbul example.) İstanbul: İstanbul Teknik Üniversitesi, Fen Bilimleri Enstitüsü, Mimarlık Anadilim Dalı, Çevre Kontrolü ve Yapı Teknolojisi, 2006.

Manioğlu G (2007) "Geleneksel Mimaride İklimle Uyumlu Binalar: Mardin'de Bir Öğrenci Atölyesi." (Climate Compatible Buildings in Traditional Architecture: A Student Workshop in Mardin.) In *VIII. Ulusal Tesisat Mühendisliği Kongresi,* 79-92. İzmir, Turkey, 2007.

Meriç Z, Manioğlu G, Akşit ŞF(2013) "Çok katlı konutların enerji korunumu açısından performansının değerlendirilmesi." (Evaluation of the performance of multi-storey houses in terms of energy conservation.) In *11. Ulusal Tesisat Mühendisliği Kongresi,* (s. 1447-1456). İzmir, 2013.

Ovalı PK (2009) *Türkiye iklim bölgeleri bağlamında ekolojik tasarım ölçütleri sistematiğinin oluşturulması "Kayaköy yerleşmesinde örneklenmesi".* (Establishing a systematic of ecological design criteria in the context of Turkey's climate zones "Exampling in Kayaköy settlement".) Edirne: T.C. Trakya Üniversitesi, Fen Bilimleri Enstitüsü, Mimarlık Anabilim Dalı, Doctoral dissertation, 2009.

Ovalı PK (2019) Biyoklimatik tasarım matrisi (Türkiye*).* (Bioclimatic design matrix (Türkiye).) *Trakya Üniversitesi Mühendislik Bilimleri Dergisi* 20, no. 2 (2019): 51-66.

Ödül H (2019) *Kentsel alanda iklimsel değişimin incelenmesi: Ümraniye örneği*. (Examining climatic change in urban areas: Ümraniye example.) Ankara: TMMOB 6. Coğrafi Bilgi Sistemleri Kongresi, 2019.

Özmen E, Beşiroğlu Ş (2020) "Aynı iklim sınıfında farklı iki ülkenin enerji etkin bina kavramı bağlamında ele alınması: İspanya ve Türkiye." (Considering two different countries in the same climate class in the context of the energy efficient building concept: Spain and Türkiye.) XIV. *Mimarlıkta Sayısal Tasarım Ulusal Sempozyumu* (2020): 129-140.

Şimşek ÇK (2020) "İstanbul'un mezo ve mikro iklimsel değişiminin kuzey ormanları ve kent içi yeşil alanlar ile ilişkisi." (The relationship of Istanbul's meso- and microclimatic change with northern forests and urban green areas.) In *Ekosistem, İklim ve Kentsel Büyüme Perspektifinden İstanbul ve Kuzey Ormanları* (s. 96-109). Türkiye Ormancılar Derneği, 2020.

Şimşek ÇK, Şengezer B (2012) İstanbul metropoliten alanında kentsel ısınmanın azaltılmasında yeşil alanların önemi. (The importance of green areas in reducing urban warming in the Istanbul metropolitan area.) *Megaron* 7, no. 2 (2012): 116-128.

T.C. Çevre ve Şehircilik Bakanlığı (2020) *Akıllı Şehir Uygulamalarında İlk Örnek Kanal İstanbul Olacak.* (Canal Istanbul will be the first example in Smart City Applications.) Ocak 2, 2021 tarihinde Türkiye Cumhuriyeti Çevre ve Şehircilik Bakanlığı: https://csb. gov.tr/akilli-sehir-uygulamalarinda-ilk-ornek-kanal-istanbul-olacak-bakanlik-faaliyet leri-29695 adresinden alındı.

T.C. Çevre ve Şehircilik Bakanlığı. *Bakan Kurum: "Kanal İstanbul Bir Devlet ve Millet Projesidir".* (Minister Institution: "Canal Istanbul is a State and Nation Project".) Ekim 22, 2021. tarihinde csb.gov.tr, 2021. https://csb.gov. tr/bakan-kurum-kanal-istanbul-bir-devlet-ve-millet-projesidir-bakanlik-faaliyetleri-30900 adresinden alındı.

Topçu C (2020) *Toplu konut planlamasında ekolojik yaklaşım önerileri Kiptaş Kayabaşı Toplu Konut Örneği.* (Ecological approach suggestions in mass housing planning Kiptaş Kayabaşı Mass Housing Example.) T.C. İstanbul Aydın Üniversitesi, Lisansüstü Eğitim Enstitüsü, Mimarlık Anabilim Dalı, Mimarlık Programı, Master's Thesis, 2020.

Turan SE (2019) *Kanal İstanbul mücavirinin mühendislik jeomorfolojisi.* (Engineering geomorphology of Canal Istanbul adjacent.) İstanbul: Marmara Üniversitesi, Sosyal Bilimler Enstitüsü, Coğrafya Anabilimdalı, Master's Thesis, 2019.

Umaroğulları F, Cihangir C (2019) Toplu konutların iklimsel konfor tasarım parametrelerine göre değerlendirilmesi: "ılıman nemli iklim bölgesi: Edirne binevler (1.kısım) konut yapı kooparetifi örneği. (Evaluation of mass housing according to climatic comfort design parameters: "temperate humid climate zone: Edirne binevler (1st part) housing building cooperative example.) *Mimarlık ve Yaşam Dergisi* 4, no.1 (2019): 105-122.

Varoğlu SE (2017) *Sıcak iklim bölgelerindeki binaların optimum yönlenme ve optimum gölgelemesi için bir yöntem.* (A method for optimum orientation and optimum shading of buildings in hot climate regions.) Yakın Doğu Üniversitesi, Fen Bilimleri Enstitüsü, Mimarlık Anabilim Dalı, Doctoral dissertation, 2017.

WWF (2015) "*Ya Kanal Ya İstanbul" Kanal İstanbul Projesinin Ekolojik, Sosyal ve Ekonomik Değerlendirmesi.* ("Either Canal or Istanbul" Ecological, Social and Economic Evaluation of Canal Istanbul Project.) İstanbul, 2015.

Athens Journal of Sciences- Volume 11, Issue 4, December 2024 – Pages 287-300

Rankings of Shorelines of Georgian Black Sea Sector According to the Ecological Sensitivity Index (ESI)

By Nino Gelashvili[*], Nino Machitadze[±], Vakhtang Gvakharia[°], Guram Maisuradze & Giorgi Beridze[•]

Georgia is concidered as one of the best alternative transit countries connecting Asia and Europe. The transportation of oil and oil products from the Caspian and Central Asian regions to European countries is especially significant. This boosts the country's economy, but it also increases the risk of marine environment pollution from oil hydrocarbons. In response to the risk of oil hydrocarbon pollution, it is necessary to intensify preventive monitoring efforts. This includes assessing the extent of oil hydrocarbon contamination on shores, in coastal waters, and in bottom sediments, as well as identifying and classifying areas along the coastline that are most sensitive to pollution. The division of shorelines into sensitive areas is carried out according to the ecological sensitivity index ESI, wich contains a numeric or alpha-numeric coded description of the shoreline characteristics for each shoreline segment. According to the 10 levels of sesitivity against oil pollution, the shoreline segments are classified from "low" sensitivity ESI 1 to "very high" sensitivity ESI 10, respectively 10 main classes and up to 30 sub-classes are identified. In Georgia coastal area, for the 113 km section from Ganmukhuri to Sarpi, we have identified shoreline segments with 7 main classes and 9 sub-classes of sensitivity.

Keywords: *Black sea, Georgia, oil, sensitivity, rankings , pollution*

Introduction

Geographical location and geopolitical situation of Georgia make it a crucial transit corridor between Asian and European countries. With the growing of volume of oil and oil products transportation from the Caspian and the Central Asian regions to Europe, there is significant international interest in the development of Georgia's transport infrastructure. Oil pipelines and transshipment terminals for oil and oil products are being built and are operational in Georgia. While this development strengthens the country's economy, it also increases the risk of pollution of marine environment with oil and oil hydrocarbons.

In response to the risks of petroleum hydrocarbon pollution, there is a need to intensify preventive monitoring studies. The monitoring activities includes assessing the pollution level of the alongshores, the coastal waters and the bottom sediments with petroleum hydrocarbons. Identifying and classifying pollution-sensitive areas

[*]Senior Scientist, Al. Janelidze Institute of Geology of I. Javakhishvili Tbilisi State University, Georgia.
[±]Senior Scientist, Al. Janelidze Institute of Geology of I. Javakhishvili Tbilisi State University, Georgia.
[°]Major Scientist, Al. Janelidze Institute of Geology of I. Javakhishvili Tbilisi State University, Georgia.
[•]Senior Scientist, Al. Janelidze Institute of Geology of I. Javakhishvili Tbilisi State University, Georgia.

along the coastline permits to assess the potential impact of an oil spill on the coastal environment.

Improving the ecological conditions of the Black sea and effectively protecting the marine environment are national obligations (Association Agreement, 2014, Directive 2008/56/EC; Convention 1992). To prevent the oil pollution of the marine environment and ensure a timely and effective response to spills, Georgia, as a signatory to the international convention OPRC 1990 (International Convention 1990), has developed the "National Plan for Response to Oil Spills at Sea" {On the approval, 2014). The plan outlines the conditions and needs arising from an oil spill in Georgia's harbors or territorial waters. It includes priorities for environmental sensitivity, details the emergency preparedness system, defines the liability and competence of the responsible persons of different level, and discusses the readness measures and actions to be implemented in the event of an oil spill. In addition to the aforementioned issues, assessing the shoreline's vulnerability using the Ecological Sensitivity Index (ESI) is both relevant and practically important tool for environmental protection. The ESI is used to evaluate the potential impact of oil spills on the coastal environment, enabling early prediction of system stability and expected changes due to external impacts. The ESI contains a numeric or alpha-numeric coded description of the shoreline characteristics for each shoreline segment (Petersen et al. 2019).

It is known that oil spilled into the hydrosphere reaches the coastline through currents, wind, and sea waves, leading to pollution. The extent of the negative impact on the coastline depends significantly on the type of coast and the ecological sensitivity of the area (Response strategy 2015). In light of the above, and to refine the sensitivity scale of the shores outlined in the national oil spill response plan, we have conducted a ranking (classification) of the Georgian sector of the Black Sea coastline using the Ecological Sensitivity Index (ESI) scale.

Study Area and Methodology

The purpose of the research was the ranking of the Georgian Black Sea coastline to assess its sensitivity against oil pollution. In case of an accidental oil spill, the sensitivity of the coastlines is determined by the many factors: relief, landscape category, beach substrate composition and grain size, geomorphological peculiarities of the shores, along-shore transport of the bottom sediments on the submarine slope, diversity and biological productivity of the coastal and marine ecosystems, recreational value of the shorelines, etc. During our research, we identified sensitive areas within the study region and assigned an index using the well used methods and the best practices (Gundlach and Hayes 1978, Petersen et al. 2019, Sensitivity mapping 2012).

According to these methods, the sensitive areas of the coastline are classified on a scale from "low" sensitivity (Class ESI 1) to "very high" sensitivity (Class ESI 10). A total of 10 main classes and up to 30 sub-classes have been identified.

The ranking is based on the shoreline sensitivity, determined by the several factors: shoreline topography, landscape category, beach substrate composition

and grain size characteristics, geomorphological features, sediment transport along the underwater slope, diversity and biological productivity of the coastal ecosystems, existing of the wetlands, the surface water bodies, and recreational value of the coastline.

The Black sea coast of Georgia, located in the eastern part of the sea, stretches for 320 km. The shores are characterized by the diversity of the landscapes and the geological features and have a high recreational value. We evaluated the sensitivity index for the central and southern section of the Georgia coastal zone from Ganmukhuri to Sarpi, which spans approximately 113 kilometers (Figure 1).

Figure 1. *The Study Area*

The Georgian coastal zone of the Black sea has an arcuate shape, convex to the east, and is comprised of three morphological units. The central unit is the Kolkheti Lowland, which is formed from the alluvium of the Rioni River and its tributaries (Kolkheti Lowland 1993). Geographically, the southern end of the Kolkheti Lowland is at the confluence of the Natanebi River, while the northern boundary is near Ochamchire. To the east, the plain is bordered by the crystalline massif of Dzhirula and to the west by the sea. It is flanked to the south by the Lesser Caucasus and Eastern Ponto mountain ranges, and to the north by the southern slopes of the Greater Caucasus (Maruashvili1971).

From a morphological perspective, the extreme southern part of the coastal zone, stretching from Cape Gonio to Kobuleti, is highly fragmented. The land relief exhibits significant variation in elevation within a small area, with deep valleys reaching heights of over 100 meters. The Adjara-Trialeti folded system in this region is predominantly composed of volcanic bedrocks, such as basalts, andesites, and tuffs, along with marine and lacustrine sedimentary formations (Kvinikadze et al. 2010).

The coastline has predominantly accumulative type, formed by sediments deposited by rivers over long geological periods. From an energetic perspective, modern lithodynamic processes - such as sediment distribution on the underwater slope and along the shores—are influenced by the sea's wave regime, currents, and gravitational forces (Gaphrindashvili et al. 2018, Zenkovich 1977). Of the total coastline, 96 kilometers (85%) are accumulative type beaches adjacent to dunes, while the ports of Batumi and Poti account for 4.5 kilometers of this length. The remaining 17 kilometers (15%) are characterized by naturally abrasive sections where beaches are absent or are limited to rocky, hard-to-erode intrusive rocks.

The sediment grain size on the beaches of the Georgian coastline ranges widely from 0.05 to 40 mm. The beaches of Kolkheti are predominantly sandy, with an average grain diameter ranging from 0.05 to 2.0 mm. In contrast, Adjara's beaches are pebbly, with an average grain diameter of 10 to 40 mm. Based on sediment grain size, the Georgian coastline is categorized into three main types: the first category includes beaches composed entirely of sandy sediments, with a total length of 43 km; the second category includes sand/shingle beaches, with a length of 30 km; and the third category comprises gravel-shingle beaches, with a length of 23 km. Additionally, in the extreme southern section of the coast near Sarpi, there is a 500-meter stretch of open rocky shores and slopes with boulders.

Among the land areas adjacent to the coastline that exhibit high ecological sensitivity and are vulnerable to pollution from oil spills, Kolkheti National Park stands out. This protected wetland area is hydrologically linked to the sea environment, including Paliastom Lake, Nabada, and Churia wetlands. Kolkheti National Park is recognized as one of the 36 biodiversity hotspots globally. The adjacent Black sea coastal aquifer features a shelf that extends an average of 6-8 km from the coastline, with wave heights ranging from 3 to 6 meters (Devidze et al. 2020). The relict swamps of Kolkheti host plant species that are now found only in the tundra and taiga wetland ecosystems of the Far North.

The territories of Kolkheti National Park are of great botanical interest. The park preserves phytocoenoses with rich assemblages of relict and endemic species, showcasing a diverse floristic composition across various plant groups, including those from swamps, marshy forests, and sandy dunes along the sea coast.

Kolkheti National Park is inhabited by 194 bird species, and many birds use the park as part of their annual migration routes: in autumn, they travel from north to south, and in spring, they move from warmer regions to their nesting sites. For some species, Kolkheti serves as a wintering area, eliminating the need for further southward migration. The park's ichthyofauna includes 88 fish species: 23 migratory, 21 freshwater, and 44 Black sea species [Assessment, 2019].

In the central part of the Kolkheti Lowlend's wetland area lies Paliastomi Lake, a unique reservoir with a surface area of 18.2 km². The lake has a maximum depth of 3.2 meters and an average depth of 2.6 meters. Located near the seashore, it is 0.3 meters below sea level. The Pichori River flows into the lake, while the Kaparchina River drains it. The Maltakva River connects the lake with the sea.

Until 1924, Paliastomi Lake was a freshwater body, sustained by atmospheric precipitation and supporting a diverse freshwater micro- and macrofauna and flora. However, after a channel was cut from the southwestern shore to the sea, the lake

became directly connected to the ocean. Over time, storm impacts widened the channel, allowing sea water to flow into the lake with little obstruction. This salinization led to significant changes in the species composition of the lake's unique fauna and flora. Despite these changes, the lake and its surroundings remain a unique ecosystem, serving as an important wintering site for migratory birds. It is also a key component of Kolkheti National Park and a notable tourist attraction.

The wetland area of Kolkheti National Park is of international significance and is protected under the Ramsar Convention (Convention on Wetlands, 1971). Its regulation and management are governed by Georgian legislation (Law of Georgia 1998/2023).

Results and Discussion

On the study area, the division of shorelines into the segments with the different level of sensitivity against oil pollution is given according to the ecological sensitivity index classes and sub-classes.

Class ESI 1

The Sub-class ESI 1A Exposed rocky shores and the Sub-class ESI 1C Exposed rocky cliffs with boulder talus base can be found in the extreme southern part of the coast of Georgia - in the vicinity of Sarpi. Taking into account wave and tidal effects, they belong to high-energy banks that directly follow the shoreline. Under the influence of prevailing winds, these shores are affected by wave action, resulting in reflected waves that carry pollution away from the shores. At the same time, the treated beach substrate is coarse-grained and easily freed from pollution. Therefore, the ecological sensitivity of these banks is low. In case of oil pollution, they will be discharged into the sea. The degree of degradation of oil and oil-contaminated waste is also high under the influence of wave disturbance (Figure 2).

Figure 2. *Sub-class ESI 1A, 1C*

Sub-class **ESI 1A** Exposed rocky shores	Sub-class **ESI 1C** Exposed rocky cliffs with boulder talus base
	
The southernmost section of the coast of Georgia - rocky shores near Sarpi (E 712622.44; N 6600327.50)	

The Sub-class ESI 1B Exposed, solid man-made structures are abundantly present in the coastal zone and can be found in the vicinity of Tsikhisdziri district, Mtsvane Kontskhi, Rion River, Shekvetili, Ureki, Tskaltsminda River. These areas are characterized by high energy and low sensitivity (Figure 3).

Figure 3. *Sub-class ESI 1B*

Sub-class ESI 1B Exposed, solid man-made structures	
	
Coastal strip in the vicinity of the Chorokhi River mouth (E 715575.50; N 4610740.87)	Coastal strip in the vicinity of Tsikhisdziri district (E 728554.50; N 4627248.05)

	
Vicinity of Shekvetili water area (E 728966.15; N 4648338.32)	Ureki, at the Tskaltsminda river mouth (E 728004.82; N 4626630.15)

The Classes ESI 3 and ESI 4

The Sub-class ESI 3A Fine- to medium-grained sand beaches and the Sub-class ESI 4 Coarse-grained sand beaches are found north of the Supsa River mouth, including Kulevi and Anaklia. The slight sloping of the beache terrain helps to disperse the wave energy and scatter the waves. The mentioned factor and the relatively high dispersion of the beach-forming material lead to a long period of natural cleaning and, accordingly, an increased sensitivity to pollution (Figure 4).

Figure 4. *Sub-class ESI 3A, 4*

Sub-class ESI 3A Fine- to medium-grained sand beaches	Sub-class ESI 4 Coarse-grained sand beaches
	
North of the Supsa river mouth, including Kulevi and Anaklia (E 727732.55; N 4655715.46 -E 710323.82; N 4696555.85) sections	

The Class ESI 5

The Sub-class ESI 5 Mixed sand and gravel beaches are present in Kobuleti-Shekvetili and Anaklia coastal strip. The shores are characterized by strong dynamism, medium slope, high degree of wave impact. Due to the large dimensions of the substrate, pollution penetrates deep into the sediment layer and fossilized, that is, they are covered with clean sediments. Fossilization is most rapid on pebbly beaches (Figure 5).

Figure 5. *Sub-class ESI 5*

Class ESI 5 Mixed sand and gravel beaches	
	
Kobuleti-Shekvetili and Anaklia coastal strip (E 7303229.70; N 4633631.20 - E 729319.70; N 4644503.79) sections	

The Class ESI 6

The Sub-class ESI 6A Gravel beaches (granules and pebbles) and ESI 6B Riprap Gravel Beaches (cobblesand boulder) - It can be found in the south and north of the Chorokhi River mouth , from Sarpi to Batumi. Taking into account the large size of the beach sediment grains, as well as the boulders present on the beaches, the probability of oil penetration and fossilization in the depth of the layer is high. Under conditions of moderate or low wave energy, oil can persist for years and hard asphalt can form. Considering this factor as well as the recreational value, the mentioned coastline is highly sensitive to pollution (Figure 6).

Figure 6. *Sub-class ESI 6A, 6B*

Sub-class ESI 6 A Gravel beaches (granules and pebbles)	Sub-class ESI 6 B Riprap Gravel Beaches (cobblesand boulder
	
The southern and northern beaches of the Chorokhi River mouth, from Sarpi to Batumi (E 714477.64; N 4609270.40 - E 719889.43; N 4615146.50 and E 712598.80; N 4600684.55)	

The Class ESI 8

The Sub-class ESI 8A Sheltered scarps in bedrock, mud, or clay Sheltered rocky shores (impermeable**)** can be found in Tsikhisdziri region and in the vicinity of Mtsvane Kontskhi. In these sections sheltered rocky shores occur. Here, due to attenuated wave action, the probability of long-term retention of spilled oil is high. These banks are also covered with dense vegetation. The ecological sensitivity of these areas is high considering the attenuated wave energy as well as the distinguished biodiversity (Figure 7).

Figure 7. *Sub-class ESI 8A*

Sub-class 8 A Sheltered scarps in bedrock, mud, or clay Sheltered rocky shores (impermeable)

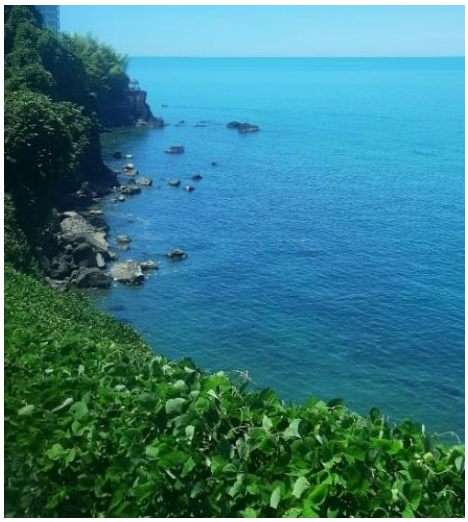

Tsikhisdziri district and Mtsvane Kontskhi
(E 728801.56; N 4627852.33 და E 728004.82; N 4626630.15)

The Sub-class ESI 8B Sheltered, solid man-made structures, Sheltered rocky shores (permeable) the mentioned category of landscape is represented by port buildings and corresponding infrastructure, which leads to relatively high sensitivity in case of spillage, due to limited water exchange (Figure 8).

Figure 8. *Sub-class ESI 8b*

Sub-class ESI 8B Sheltered, solid man-made structures Sheltered rocky shores (permeable)	
	
Poti sea port (E 718964.70; N 4670495.09)	Batumi sea port (E 720895.36; N 4614345.5)
	
Kulevi sea port (E 717337.82; N 4683293.49)	Batumi Coast Guard Marina (E 723088.49; N 4615874.76)

Class ESI 10

The Sub-class ESI 10C Swamps - Swamps are present in the coastal strip of Poti-Anaklia. This section is distinguished by the highest sensitivity: it represents the wetland area of the Kolkheti plain, here there are coastal marshes characterized by a low rate of water exchange and a high indicator of ecological criteria of sensitivity - dense vegetation and a large number of habitats (Figure 9).

Figure 9. *Sub-class ESI 10C*

Sub-class ESI 10 C Swamps

Wetlands of Kolkheti plain Poti-Anakli - (E 717139.00; N 4684150.90 - E 713935.17; N 4693363.77) sections

The results of the study showed that taking into account the type of beach, beach substrate and ecological factors in case of the oil spills, the most sensitive area of the Georgian coastline of the Black sea is the wetlands of the Kolkheti plain with a sensitivity index of ESI 10 C (Figure 10). Paliastomi Lake, hydrologically connected to the sea environment, is located in the mentioned area. Carrying out pollution elimination works will be associated with significant difficulties, and it is problematic to predict the results. It should also be taken into account that the mentioned area belongs to the wetland territory of the Kolkheti National Park, which is of International importance and is protected by the Ramsar Convention, and its regulation and management is determined by the legislation of Georgia [17,18].

Figure 10. *Paliastomi Lake*

Paliastomi Lake (E 725461.07; N 4666822.81)

Tsikhisdziri district and Mtsvane Kontskhi are also highly sensitive to the impact of an accidental oil spill, with a sensitivity index of ESI 8A. Due to the

covered rocky shores and the (attenuated) low rate of wave action in these sections, the probability of long-term retention of spilled oil is high. These banks are also covered with dense vegetation.

Considering the type of substrate (gravel) and recreational purpose, the Adjara section is also highly sensitive with a sensitivity index of ESI 6A. It should be noted that the shores in this section are highly dynamic, characterized by a medium slope and significant wave impact. Due to the large size of the substrate (pebbles), pollution can penetrate deeply into the sediment layer and become buried, with clean sediments covering them from above. Fossilized oil layers we identified were described during the construction of the Batumi Coast Guard pier (Gelashvili et al. 2020). Our research, both completed and planned, is crucial as it introduces a new risk factor for oil pollution: oil exploration activities in both river basins that flow into the sea and the sea shelf area. Based on our research data, we will prepare Ecological Sensitivity Index (ESI) maps of the coastal zones of Black sea Georgia using geoinformation systems (GIS).

Conclusions

The results of the study showed us that taking into account the type of beach, beach substrate and ecological factors in case of oil spills, the most sensitive area of the Georgian coastline of the Black sea is the wetlands of the Kolkheti plain with a sensitivity index of ESI 10 C. Paliastomi Lake, hydrologically connected to the sea environment, is located in the mentioned area. Carrying out pollution elimination works will be associated with significant difficulties, and it is problematic to predict the results.

The most sensitive area of the coastline is the wetlands of the Kolkheti Lowland, with a higher sensitivity index ESI 10C. These coastal wetlands are characterized by a low rate of water exchange procrsses and a high ecological sensitivity index due to dense vegetation and a large number of habitats. It should also be taken into account that the mentioned area belongs to the wetland territory of the Kolkheti National Park, which is of International importance and is protected by the Ramsar Convention, and its regulation and management is determined by the legislation of Georgia.

Tsikhisdziri district and Mtsvane Kontskhi are also highly sensitive to the impact of an accidental oil spill, with a sensitivity index of ESI 8A. Due to the covered rocky shores and the (attenuated) low rate of wave action in these sections, the probability of long-term retention of spilled oil is high. These banks are also covered with dense vegetation.

Considering the type of substrate (gravel) and recreational purpose, the Adjara section is also highly sensitive with a sensitivity index of ESI 6A, due to its gravel substrate and recreational use.

Acknowledgments

Our thanks to our colleagues at the scientific team of Ltd Research Center GAMMA and GAMMA Consulting (Tbilisi, Georgia) for their assistance in the field works. We would like express our sincere gratitude to Dr. Guram Maisuradze to and engagement in the study research, posthumously.

References

Association Agreement between the European Union and the European Atomic Energy Community and their Member States, of the one part, and Georgia, of the other part (2014) Oficial Journal of the European Union 30.8.2014. L 261/579. Annex XXVI Environment.

Convention on the Protection of the Black Sea Against Pollution (1992) Bucharest Convention.

Convention on Wetlands of International Importance, especially as Waterfowl Habitat (1971) Ramsar, 2.2.1971.

Devidze M, Machutadze I, Pirosmanashvili M (2020) *Wetlands of Kolkheti plain and their pollution sources*. Eco-Conscious Minds to Save the Valuable Wetland Environment of the Black Sea – Biolearn, Tbilisi, 1–28.

Directive 2008/56/EC of the European Parliament and of the Council of 17 June 2008 (2008) *Establishing a framework for community action in the field of marine environmental policy* (Marine Strategy Framework Directive).

Gaphrindashvili N (2019) *Assessment of Geomorphological and Geodynamic Changes and Risks Regarding to Development of Marine Infrastructurein the Black sea coast of Georgia*. Doctoral Thesis. St. Andrew the First-Called Georgian University of the Patriarchate of Georgia.

Gaphrindashvili N, Papashvili I, Machitadze N, Gelashvili N, Gvakharia V (2018) Assessment of Lithomorphodynamic Status of Batumi - Gonio Coastline. *Georgia Chemical Journal* 18(1): 223–228 (In Georgian).

Gelashvili NE, Maisuradze GV, Janashvili ND, Machitadze NO, Gaprindashvili NG, Gvakharia VG (2020) Level of Oil Hydrocarbons and Their Distribution within the Deep Layers of Bottom Sediments of Batumi Coast Guard Harbor and the North Part of Port of Poti. In *The International Scientific Conference "Environmental Protection and Sustainable Development" dedicated to Professor Victor Eristavi's Memory*. (Tbilisi, Georgia). 254–255. (In Georgian).

Gundlach ER, Hayes MO (1978) Vulnerability of Coastal Environments to Oil Spill Impacts. *Marine Technology Society Journal* 12: 18–27.

International Convention on Oil Pollution Preparedness, Response and Co-operation (OPRC 1990).

Kolkheti Lowland. Natural conditions and social-economic aspects (1993) Leningrad, Hydrometeoizdat 373–410. (In Russian).

Kvinikadze M, Kuparadze D, Pataridze D, Khundadze N, Kirakosyan V (2010) *Geoecology of the Black sea Coast of Georgia*. Scientific Annals, School of Geology, Aristotle University of Thessaloniki Proceedings of the XIX CBGA Congress, (Thessaloniki, Greece), 100, 97–103.

Law of Georgia (1998/2023) *About creation and management of protected areas of Kolkheti*. (In Georgian).

Maruashvili LI (1971) *Geomorphology of Georgia*. Tbilisi, Metsniereba 1–609. (In Russian).

On the approval of the national plan for responding to oil spills in the sea. Ordinance of the Government of Georgia 195, 22/04/2016. (In Georgian).

Petersen J, Nelson DM, Marcella T, Michel J, Atkinson M, White M, et al. (2019) *Environmental Sensitivity Index Guidelines*. Version 4.0. U.S. Department of Commerce National Oceanic and Atmospheric Administration (NOAA) National Ocean Service - Office of Response and Restoration Emergency Response Division. Technical Memorandum NOS OR&R 52 April 2019.

Response strategy development using net environmental benefit analysis NEBA (2015) *Good practice guidelines for incident management and emergency response personal. The global oil and gas industry association for environmental and social issues and emergency response personnel IPIECA*. International Association of Oil & Gas Producers.

Sensitivity mapping for oil spill response Good practice guidelines for incident management (2012) *The global oil and gas industry association for environmental and social issues and emergency response personnel IPIECA*. International Maritime Organization IMO; International Association of Oil & Gas Producers.

Zenkovich VP (1977) The problem of stability of sea coasts in the Georgian. *SSR. Geomorfology* 1: 50–54. (In Russian).